Contract No:

This document was prepared in conjunction with work accomplished under Contract No. 89303321CEM000080 with the U.S. Department of Energy (DOE) Office of Environmental Management (EM).

Disclaimer:

Review of Residual Stresses in Spent Nuclear Fuel Canisters

Spent Fuel and Waste Disposition

Prepared for
U.S. Department of Energy
Spent Fuel and Waste Science and Technology

Xian-Kui Zhu
Robert L. Sindelar
Savannah River National Laboratory

August 19, 2022

Milestone No. M4SF-22SR010207084
SRNL-STI-2022-00395

Prepared by
Savannah River National Laboratory
Aiken, South Carolina 29808

Savannah River National Laboratory is a multiprogram laboratory managed and operated by Battelle Savannah River Alliance, LLC, for the U.S. Department of Energy under Contract No. 89303321CEM000080.

EXECUTIVE SUMMARY

This report compiles the set of published results on the welding residual stress (WRS) distributions across the thickness section at the welds in spent nuclear fuel (SNF) canisters before and after a repair is done. The WRS information for similar steel structures with thick (~ 12.7 mm (0.5 inch)) large plate construction are also compiled to provide a comprehensive set of information on: methods to quantify; modeling to estimate; and methods to reduce WRS.

The WRS can impact canister integrity in two modes: i) WRS provides the tensile stress to drive chloride-induced stress corrosion cracking (CISCC); and ii) WRS can impose stresses on a crack that can reduce the mechanical stability of a crack in the canister. It is therefore important to quantify the WRS in a canister to be able to evaluate subcritical crack growth and mechanical stability of a crack to establish the ability of a canister to maintain leak integrity and structural integrity, respectively, for canister aging management.

Measurements of WRS in a specific prototypical SNF canister from Sandia National Laboratory (SNL) (mock-up canister) have been previously reported and the results are reproduced herein. The estimation of the WRS from consensus code prescribed methods, and from modeling of the welding process for this prototypical SNF canister have been previously performed in the program and the results are reproduced herein.

Repair method(s) for a canister are being developed to eliminate the potential for surface cracking and/or to mitigate the continued growth of a crack from CISCC in SNF canisters. Literature information on the repair methods and their impact to WRS are summarized herein.

This report summarizes the WRS profiles in canister weldments from published work in the following areas:

- Residual stress determination for as-welded canisters

  For the as-welded canisters, three methods can be used to determine the WRS: API 579 estimation procedures; Finite Element Analysis (FEA) simulation; and experimental measurements with Deep Hole Drilling (DHD), neutron diffraction, or contour method. With the residual stresses, the crack driving force, described by the stress intensity factor, and the crack instability assessment can be performed using the API 579 procedures.

- Non-welding repair methods for CISCC and to reduce WRS for canisters

  To reduce or relieve the WRS in canisters, three repair methods/post-weld treatments may be applied on the arc welds in the canisters: cold spray; laser peening; and local post-weld heat treatment (local PWHT). Those post-weld treatment technologies have been demonstrated effective for reducing or relieving the WRS in a canister and thus for avoiding crack formation in the welds.

- Welding repair methods to provide a repair equivalent to as-fabricated canisters with additional benefit of reduced/eliminated WRS

  Structural repair methods to return the canister to full net section dimensions are limited to weld methods. Two weld repair approaches can be used to structurally repair cracks and to reduce/eliminate residual stresses: fusion welding and Friction stir welding (FSW).

Recommendations are made for developing optimized welding process to reduce WRS, for improved methods for estimating WRS for crack instability criteria, and for additional post-fabrication treatment or repair methods, such as laser peening, mechanical patch and reinforced sleeves.

This report fulfills the M4 milestone M4SF-22SR010207084, "Evaluation of structural impact to flawed canister for candidate repair methods" under Work Package Number SF-22SR01020708, Rev. 1.

ACKNOWLEDGMENTS

The authors gratefully acknowledge the support of Ned Larson, U.S. Department of Energy, Office of Nuclear Energy, Office of Spent Fuel and Waste Disposition, Office of Spent Fuel & Waste Science and Technology, for sponsorship of this work. The work on Weld Residual Stresses and canister repair methods from the national laboratory teams by Charles Bryan at SNL and Ken Ross at PNNL provided key information in this report. The previous work of our colleague Poh-Sang Lam and our associates at Korea University also provided key information in this report.

This page intentionally blanked.

Table of Contents

List of Figures

List of Tables

List of Nomenclature

σ^r	Welding residual stress
$\sigma(x)$	Stress distribution on crack surface at local coordinate x
$\sigma_0 - \sigma_4$	Stress coefficients of stress distribution $\sigma(x)$
σ_b	Bending stress
σ_m	Membrane stress
σ_{ys}	Yield strength
σ^r_{ys}	Effective yield strength for estimating residual stress
Φ	Plasticity interaction factor
a	Crack depth of semi-elliptical surface crack
2c	Crack length of semi-elliptical surface crack
D	Diameter
D/t	Diameter to wall thickness ratio
E	Elastic modulus
G0, G1	Stress intensity factor influential factors
G2, G3, G4	Stress intensity factor influential factors
J	J-integral
K	Stress intensity factor
K_I^P	Primary stress intensity factor
K_I^{SR}	Second stress intensity factor
K_{Ic}	Fracture toughness in the elastic conditions
K_{Iscc}	Fracture toughness for SCC
P	Internal pressure
R_r	Reduction in WRS related to the test pressure
r/t	Radius to wall thickness ratio
t	Wall thickness
x	Local coordinate at the surface crack

List of Acronyms

API	American Petroleum Institute
ASME	American Society of Mechanical Engineers
AW	As-welded
BPVC	(ASME) Boiler and Pressure Vessel Code
CISCC	Chloride induced stress corrosion cracking
CS	Cold spray
DOE	Department of Energy
DCSS	Dry cask storage system
DHD	Deep hole drilling
ECA	Engineering Critical Analysis
EDM	Electrical discharge machining
EPFM	Elastic-Plastic Fracture Mechanics
EPRI	Electric Power Research Institute
FAD	Failure Assessment Diagram
FEA	Finite Element Analysis
FFS	Fitness For Service
FSW	Friction Stir Welding
FZ	Fusion zone
GMAW	Gas metal arc welding
GTAW	Gas tungsten arc welding
HAZ	Heat affected zone
ID	Inside Diameter
iDHD	incremental Deep Hole Drilling
ISFSI	Independent spent fuel storage installations
KU	Korean University
LEFM	Linear Elastic Fracture Mechanics
MPC	Multipurpose Canister
ND	Neutron Diffraction
NLFM	Non-Linear Fracture Mechanics
NRC	Nuclear Regulatory Commission
OD	Outside Diameter
ORNL	Oak Ridge National Laboratory
PNNL	Pacific Northwest National Laboratory
PTW	Part-Through Wall
PVP	Pressure Vessel and Piping
PWHT	Post-Weld Heat Treatment
R&D	Research and Development
RS	Residual stress
SAW	Submerged Arc Welding
SCC	Stress Corrosion Cracking
SIF	Stress Intensity Factor
SNF	Spent Nuclear Fuel
SNL	Sandia National Laboratories
SMTS	Specified Minimum Tensile Stress
SMYS	Specified Minimum Yield Stress

SRNL	Savannah River National Laboratory
SZ	Stir Zone
SS	Stainless Steel
TW	Through-Wall
U.S.A.	United States of America
UTS	Ultimate Tensile Stress
WRS	Welding Residual Stress
WT	Wall Thickness
YS	Yield Stress
3D	Three Dimensional

1. Introduction

Stainless steel (SS) spent nuclear fuel (SNF) canisters deployed in dry storage systems were fabricated by fusion welding. Post-Weld Heat Treatment (PWHT) for relieving the Weld Residual Stresses (WRS) is not required during canister fabrication. As a result, early studies acknowledged that SNF canisters may be susceptible to Chloride Induced Stress Corrosion Cracking (CISCC) in marine environments where deliquescent salts may deposit on the surface [1-3].

Under WRS alone, surface cracks may initiate, and the subsequent subcritical crack growth may lead to a through wall (TW, leakage) crack [4-5]. Additionally, the WRS mechanically-loads the crack and affects its stability. This impact to the confinement boundary was recognized by the nuclear community. As requested by the U.S. Nuclear Regulatory Commission (NRC), an ASME SC XI code case N-860 [6] was prepared to provide an aging management program for SNF canisters in extended storage. The technical bases for the code case included a suggested crack growth rate model and a flaw tolerance evaluation [7] to support the ASME code case N-860. Codification of canister repair/remediation methods are being developed by ASME SC XI [8], and these methods may alter the WRS from the original as-fabricated canister.

The objective of this present report is to review and compile the published results on the WRS distributions in SNF canisters before and after a repair and/or stress-relief treatment would be done. Estimation methods, measurements, and modeling of WRS are included. Previous work is replicated for completeness to provide a single-source topical report on canister WRS. Emphasis is given to the flaw stability of WRS-loaded flaws.

2. Multi-Purpose Canisters and API 579 Estimation of Residual Stresses

2.1. Geometry of Canisters

Various canister designs have been used to store spent nuclear fuel at ISFSIs. This work focuses on the Holtec International Storage Module (HI-STORM) that was selected by Lam and Sindelar [5] for the calculation of instability crack sizes that were employed to develop flaw acceptance criteria for the structural integrity assessment of canisters. The Multipurpose Canister (MPC) is a cylindrical vessel with all components made of austenitic SS (typically, 304 SS). The canister height is 4.8 m (189 in.) with an outside diameter (OD) of 1.73 m (68.11 in.) and a wall thickness (WT) of 12.7 mm (0.5 in.), leading to OD/WT = 136.2. The inside diameter (ID) of the vessel is 1.705 m (67.11 in).

The cylindrical vessel is constructed with one circumferential (girth) weld at the mid-height and four axial (seam) welds in the upper and lower parts, as shown in Figure 1. The upper and lower axial welds are offset slightly along the circumferential weld. The cylindrical shell is welded to a bottom plate with a thickness of 63.5 mm (2.5 in.). Submerged arc welding (SAW) with full penetration was applied. Although a post-weld nondestructive inspection is carried out, the PWHT to relieve WRS is not required for the construction. Flaw stability criteria were developed for postulated cracks in the heat affected zone (HAZ) at these critical weld locations [5].

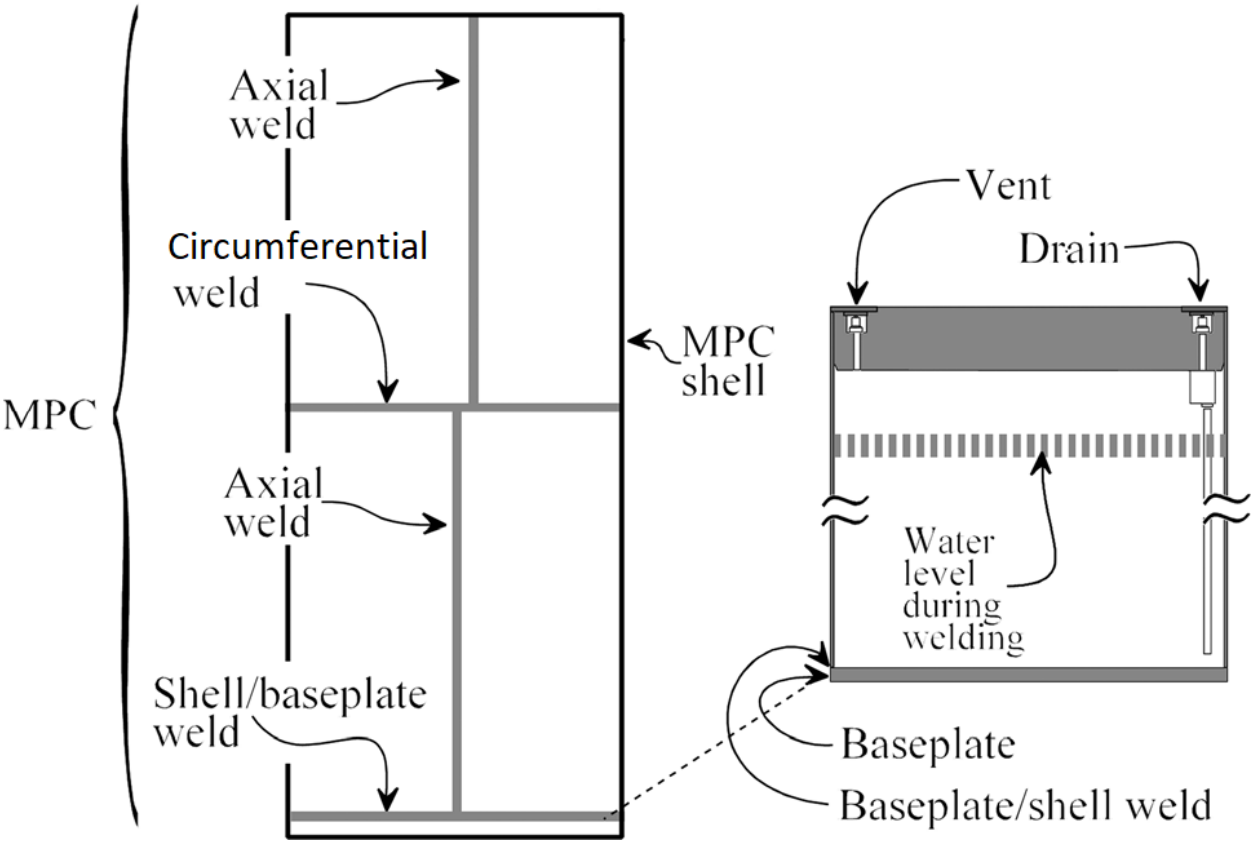

Figure 1 - Illustration of multi-purpose canister and welds. The image on the right depicts the water level (near the canister top) during lid closure welding

2.2. Loading of Canisters

The SNF assemblies are loaded vertically into the canister. The total weight of the loaded canister is about 36 metric tons or 40 short tons, see Table 1. The closure welds in the lid region were not considered in the MPC failure assessment because (1) GTAW in the lid region are tougher than the SAW in the canister shell and the baseplate; (2) multiple layers of welds between the closure ring and shell and between the lid and shell provide redundant safety features for the lid; and (3) lower stresses under normal and accident loads are expected in the lid [9]. Therefore, flaw stability criteria were not developed for closure welds.

The loading conditions that are used to calculate the instability crack sizes are listed in Table 1. Both normal and accident conditions are included. They are identical to those employed in the previous flaw tolerance analysis based on the limit load [5].

Table 1 - Load cases for canister HI-STORM

Loading case	Design internal pressure, MPa (psig)	Loaded canister mass, kg (kips)	Axial handling load or acceleration
Normal conditions	0.69 (100)	40,800 (90)	1.15 g
Accident conditions	1.38 (200)	40,800 (90)	1.15 g

2.3. Welding Residual Stresses in Canisters

Four flaw configurations as shown in Figures 2-5 in the HAZ are considered: Case (1) Axial crack parallel to an axial weld with dominant WRS perpendicular to the weld (to open the crack), Case (2) Axial crack perpendicular to a circumferential (girth) weld with dominant WRS parallel to the weld, Case (3) Circumferential crack parallel to circumferential weld with dominant WRS perpendicular to the weld, and Case (4) Circumferential crack perpendicular to an axial weld with dominant WRS parallel to the weld. Note that in the figures, RS denotes residual stress, Linear denotes linear stress distribution, and Self Equilib denotes self equilibrium of residual stress. The respective WRS were estimated by API 579 procedures. The major inputs for the WRS calculations recommended in API 579 Annex E - *Residual Stress in a Fitness-for-Service Evaluation* [10] include the following aspects:

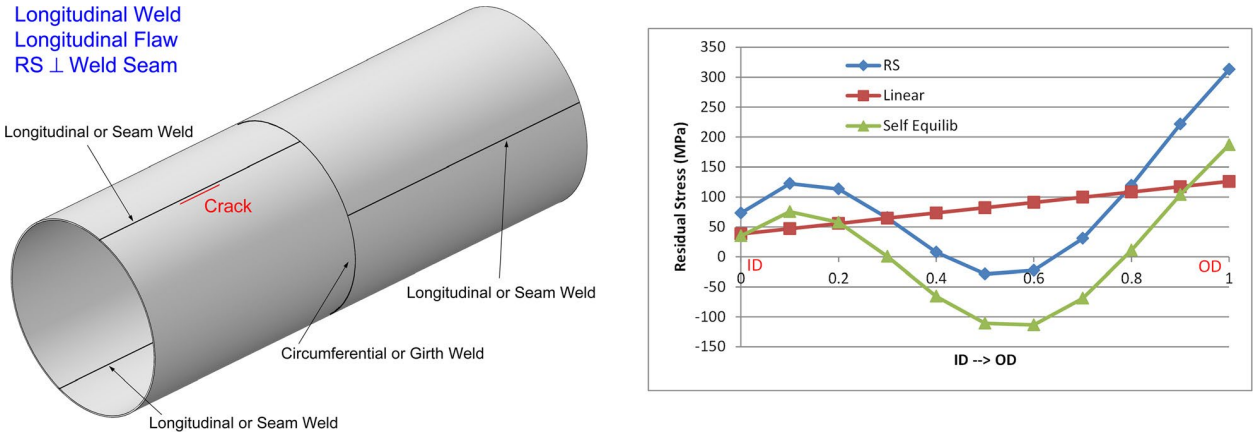

Figure 2 – Case 1: axial crack parallel to an axil weld – WRS perpendicular to the axial weld with a double-V notch

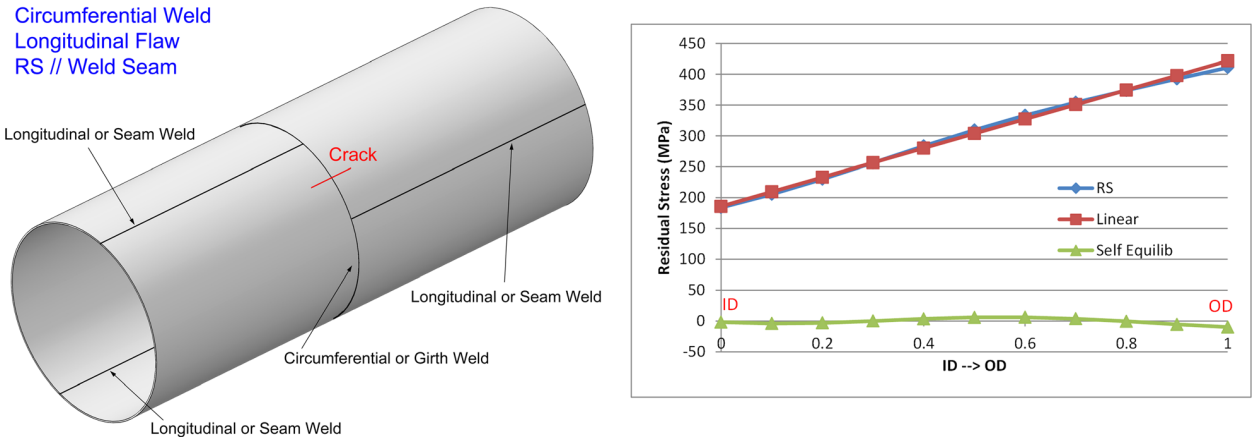

Figure 3 - Case 2: axial crack perpendicular to a circumferential weld – WRS parallel to the circumferential weld with a double-V notch

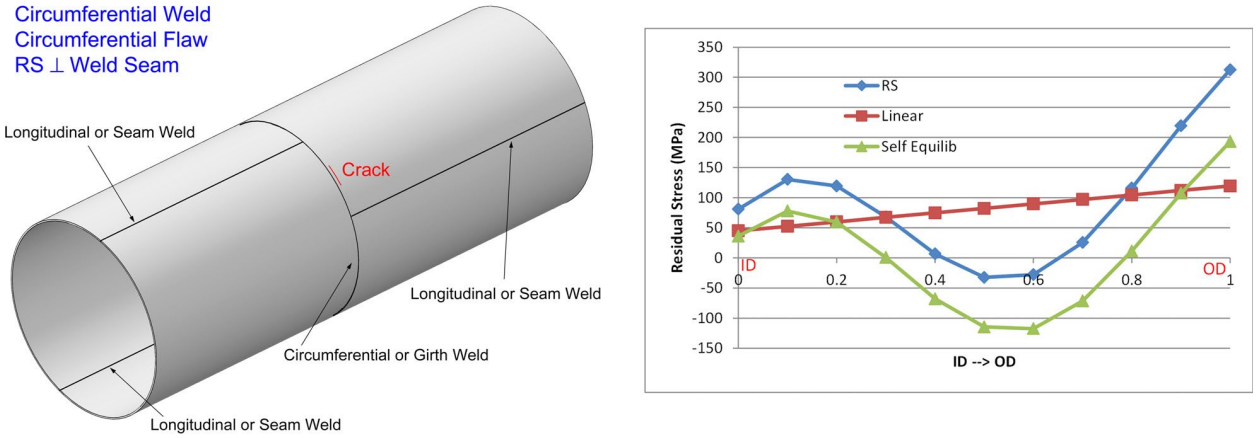

Figure 4 - Case 3: circumferential crack parallel to a circumferential weld - WRS perpendicular to the circumferential weld with a double-V notch

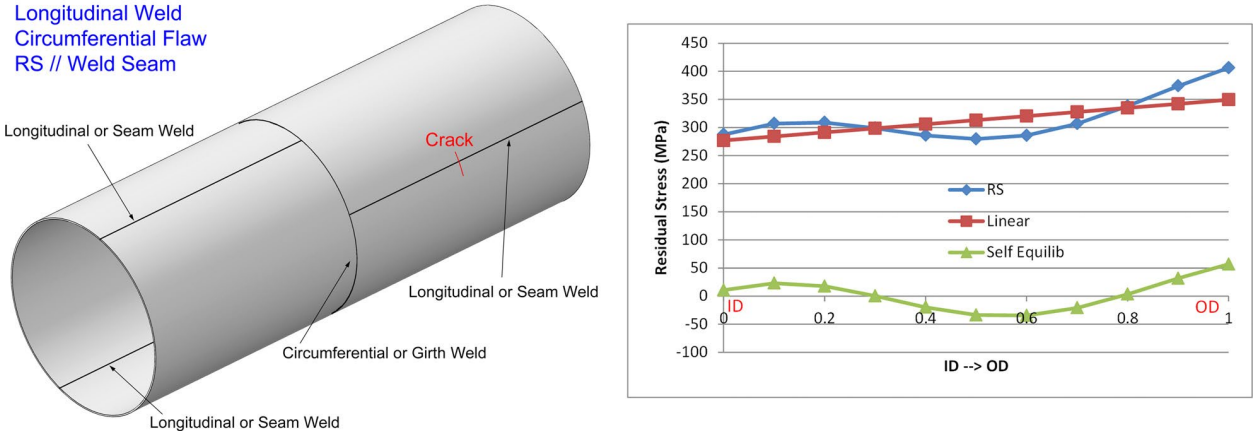

Figure 5 - Case 4: circumferential crack perpendicular to an axial weld – WRS parallel to the axial weld with a double-V notch

(1) **Yield Stress** – If an actual yield strength is not available, the yield stress (YS) used to estimate the WRS is $\sigma_{ys}^{r} = \sigma_{ys} + 69\ MPa$ (or is $\sigma_{ys}^{r} = \sigma_{ys} + 10\ ksi$), where σ_{ys}^{r} is the effective yield strength used to estimate the WRS, and σ_{ys} is the specified minimum yield strength (SMYS) of the material. From ASME BPVC, Section II, Part D, the SMYS for 304 SS is 205 MPa (30 ksi) and the minimum specified ultimate tensile strength (SMTS or UTS) is 515 MPa (75 ksi). Note that for the current analysis with API 579 Level 2 or 3 assessment, the flow stress, and thus the UTS, is not used.

(2) **Welding Parameter** – API 579 Annex E provides estimation equations for calculating the membrane and bending stress components of the WRS. The key input parameter is the heat input density ($\hat{Q}$), which is a linear function of the heat input to the weld. However, the welding parameters are proprietary information and not available for public dissemination. Thus, API 579 Annex E suggested value of 1080 J/mm is selected as the average heat input in the analysis. API 579 also provides an upper bound heat input of 1920 J/mm.

(3) **Residual Stresses (RS)** – Once the heat input density parameter $\hat{Q}$ is determined, API 579 Annex E Sections E.4.2 (double V-groove circumferential welds) and E.4.4 (double V-groove longitudinal welds) provide the equations for the estimated residual stress (RS) parameters $\bar{\sigma}_m^r$, $\bar{\sigma}_b^r$, s_0^r, and s_i^r, where $\bar{\sigma}_m^r$ and $\bar{\sigma}_b^r$ are the normalized membrane and bending stress components of the WRS, respectively, $s_0^r = K - |\bar{\sigma}_m^r| - |\bar{\sigma}_b^r|$ and $s_i^r = 0.25 s_0^r$, in which K=1.2 or 1.5, depending on whether the WRS is perpendicular or parallel to the weld, respectively. These parameters are the polynomial functions of $\hat{Q}$ and $\bar{R}$ ($\bar{R} = r/t$, where r is the vessel mean radius, and t is the nominal vessel thickness, but $\bar{R} = 30$ when r/t < 30). From API 579 Annex E, the WRS (σ^r) across the thickness of the vessel wall is given as:

$$\sigma^r(x/t) = \hat{E}\sigma_{ys}^r R_r \quad (1)$$

Where E is a position-dependent WRS factor, R_r is the reduction in WRS related to the test pressure, and x is measured from the vessel inside wall. For the present analysis, $R_r = 1.0$.

Through thickness RS for the canister wall for the four flaw configurations, calculated from Equation (1), are shown in Figures 2-5. These figures also show the variations of the linear and the self-equilibrating parts of the WRS through the thickness of the canister wall. Each of the WRS distribution is fitted with a fourth-order polynomial (Table 2), and its coefficients (σ_0, σ_1, σ_2, σ_3, and σ_4) can be used to calculate the stress intensity factor (SIF) based on API 579 Annex C – *Compendium of Stress Intensity Factor Solution*. These stress coefficients may also be used for calculating the reference stress, but instead the membrane and bending parts of the WRS are often conveniently used given the simple form of the equations.

Table 2 - Coefficients of the 4th-order polynomial for through - thickness WRS distribution

Case	σ_0 (MPa)	σ_1 (MPa)	σ_2 (MPa)	σ_3 (MPa)	σ_4 (MPa)
1	314.60	-790.83	-2248.35	7081.99	-4288.01
2	410.99	-190.54	91.54	-339.02	211.26
3	314.13	-800.73	-2323.15	7317.54	-4430.58
4	406.69	-286.26	-683.33	2150.36	-1303.24

2.4. Determination of Crack Acceptance Criterion

With the applied loadings to a canister and the estimated WRS for a specific crack, the instability crack sizes can be determined using the Failure Assessment Diagram (FAD) method as recommended by API 579, where the yield stress σ_{ys} = 205 MPa (30 ksi) and fracture toughness K_{Ic} = 207 MPa√m for the HAZ of 304 SS at temperature of 125 ºC. Note that this elastic fracture toughness K_{Ic} was converted from the elastic-plastic fracture toughness J_{Ic} obtained from the J-R curve testing with 0.394T CT specimens in the C-L direction.

From the loading conditions in Table 1 for the canister, the primary loadings involve only the internal pressure (p), the deadweight (normal), and the axial handling or acceleration (accident). The net section bending moments (M) and the crack face pressure (p_c) are not considered as the primary loading. In contrast, the secondary loading or WRS does have a bending component, and so appropriate equations must be used. As discussed earlier, the WRS is typically expressed as a

fourth-order polynomial (e.g., Table 2), or expressed by the combination of a membrane stress σ_m and a bending stress σ_b in the forms of:

$$\sigma_m = \sigma_0 + \frac{\sigma_1}{2} + \frac{\sigma_2}{3} + \frac{\sigma_3}{4} + \frac{\sigma_4}{5} \quad (2)$$

$$\sigma_b = -\frac{\sigma_1}{2} - \frac{\sigma_2}{2} - \frac{9\sigma_3}{20} - \frac{2\sigma_4}{5} \quad (3)$$

For the primary loading, the primary stress intensity factor K_I^P is calculated. For the secondary loading, the secondary stress intensity factor K_I^{SR} is calculated by following API 579 K estimation procedures. The total SIF or K_I for a crack in a weld of canisters is superposed as:

$$K_I = K_I^P + \Phi K_I^{SR} \quad (3)$$

where Φ is a plasticity interaction factor and introduced as a function of the primary and secondary (WRS) loads.

The instability crack size is determined at the intersection point of the assessment locus (crack driving force) and the FAD failure curve (fracture resistance). This point defines the instability crack length or depth for a crack under a given load with or without WRS. In comparison with the flaw tolerance determined previously by Chu [4] using the limit load or net section yielding approach, a significant reduction in the instability crack size was observed by the consideration of WRS within the FAD analysis framework.

Through detailed analysis and comparisons, Lam and Sindelar [5] showed the significant effects on the instability crack sizes due to the WRS, the orientation of the crack with respect to the weld, and the direction of the WRS. As such, the WRS should be included in the analysis as a secondary load (stress).

3. Residual Stress Estimation by API 579 Procedures

3.1. Residual Stress Estimation for Through-Wall Cracks

Lam et al. [11] proposed the framework to develop flaw acceptance criteria for structural integrity assessment of MPC for extended storage of SNF in terms of API 579 crack assessment procedures. On this basis, Lam and Sindelar [5, 12] performed detailed TW crack instability analysis with consideration of WRS for an MPC, as described in Sections 2.3 for the WRS distribution estimation cross the wall thickness and in Section 2.4 for the crack instability analysis and the flaw acceptance criterion analysis.

The WRS play are the primary stress contributor to CISCC. Thus, the total applied K factor or the J-integral must include the contribution from the WRS. API 579 Annex E was used for estimating the WRS. Because it is recommended for ferritic and stainless-steel weldments, the API equations are suitable for MPC welds.

3.2. Stress Intensity Evaluation for Surface Cracks

Shi et al. [13] extended the canister flaw assessment by Lam and Sindelar [5, 10] by considering the semi-elliptical surface flaws to estimate stress intensities more rigorously than those using the

simplified TW and part through wall PTW crack configurations. The British FF code R6 Option 1 fracture assessment procedure [14] was adopted to evaluate flaw sta, which is equivalent to the API 579 Level 2 procedure used previously by Lam and Sindelar [5, 12].

The loading conditions and the WRS distributions developed by Lam and Sindelar [5] are considered. Four outside semi-elliptical crack configurations in the HAZ, that are similar to TW cracks in Figures 2-5, were considered for developing the surface flaw instability lengths and depths: RS1 is similar to Case 1 in Figure 2, RS2 is similar to Case 2 in Figure 3, RS3 is similar to Case 3 in Figure 4, and RS4 is similar to Case 4 in Figure 5. Figure 6 shows the TW distributions of WRS for these four surface cracks that were obtained by Lam and Sindelar [5]. These WRS distributions may differ from actual measurements or estimates by other codes like R6 or BS 7910. For 304 SS, the minimum YS is 205 MPa (30 ksi), and the minimum UTS is 525 MPa (75 ksi).

For the axial and circumferential, outside, semi-elliptical surface cracks, the K factors are calculated in the following polynomial equations provided in R6:

$$K_I = \sqrt{\pi a}\sum_{i=0}^{3}\sigma_i f_i\left(\frac{a}{t},\frac{2c}{a},\frac{R_i}{t}\right) \tag{4}$$

$$K_I = \sqrt{\pi a}\left(\sum_{i=0}^{3}\sigma_i f_i\left(\frac{a}{t},\frac{2c}{a},\frac{R_i}{t}\right) + \sigma_{bg} f_{bg}\left(\frac{a}{t},\frac{2c}{a},\frac{R_i}{t}\right)\right) \tag{5}$$

Where a is the crack depth, 2c is the crack length, R_i is the inside radius of the vessel, t is the wall thickness, σ_{bg} is the global bending stress, the tubulated values of f_i and f_{bg} are given in R6 [14].

Figure 7 shows the estimated K results for the four surface crack cases due to (1) the WRS alone, (2) combined WRS and the primary loads under normal conditions, and (3) combined WRS and the primary loads under accident conditions. It shows that the WRS component parallel to the weld (RS2) plays a more important role in crack initiation than the WRS component perpendicular to the weld. With the K solutions, from the FAD analysis, the critical crack length and depth can be obtained.

3.3. Bounding Residual Stress Estimation for Surface Crack

Lam et al. [15] discussed the PTW crack perpendicular to the circumferential welds on the outside surface of a SNF canister that has been shown to be the most limiting fracture configuration driven by the WRS. A series of semi-elliptical cracks of various sizes is chosen to calculate the K factors under a bounding WRS (i.e., the stress distribution that bounds all WRSs in a canister), as shown in Figure 8. The threshold K factor (K_{ISCC}) of the canister material in the storage environment is used to determine the flaw size at K_{ISCC}, below which the SCC growth would not be expected to occur.

The canister flaw acceptance criteria developed by Lam and Sindelar [5] and Shi et al. [13] for PTW surface cracks in a canister under the influence of WRS and applied external loads are part of the options [7] for flaw disposition for the ASME BPVC Code Case N-860. The work by Lam et al. [14] focused on CISCC to establish a threshold SIF K_{ISCC} and the acceptable initial flaw size below which the SCC growth will not take place. The results were also input to Code Case N860.

The actual measurements of WRS at Sandia [16] are consistent with those estimated by Lam and Sindelar in the guideline of API 579 Annex E [10]. For simplicity, they adopted the K solution for a semi-elliptical, outside surface crack in a flat plate developed by Newman and Raju [17] as an approximation. Then they obtained the critical surface crack length and depth.

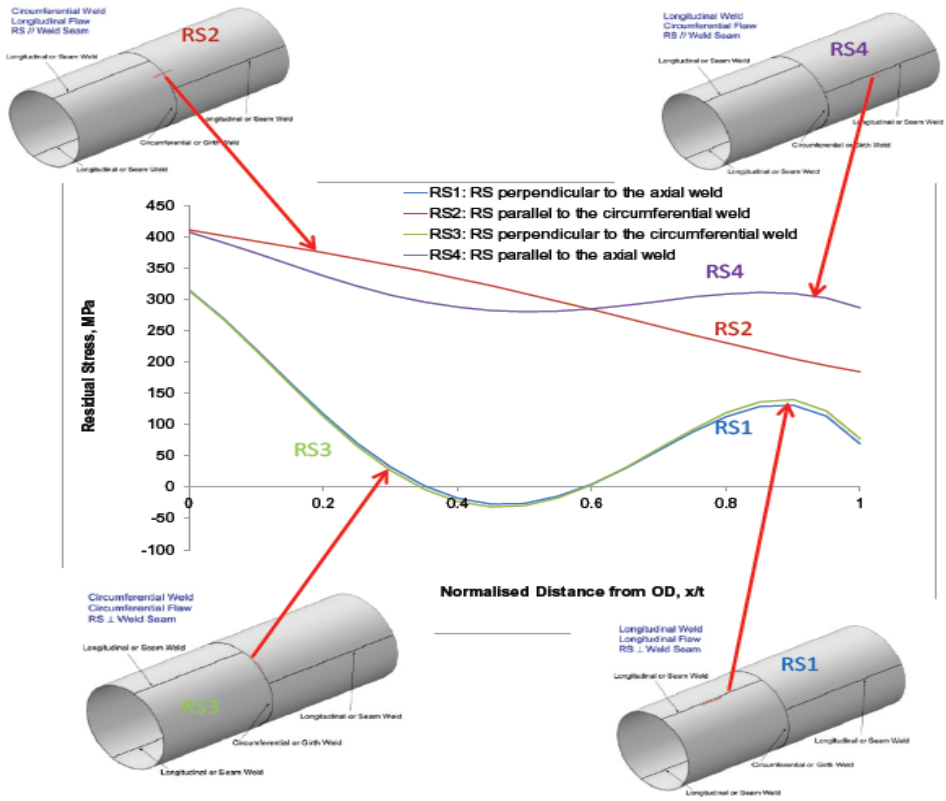

Figure 6 - Residual stress distributions for four crack cases

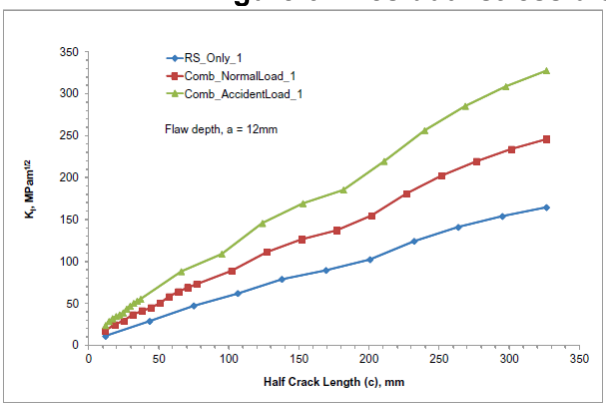

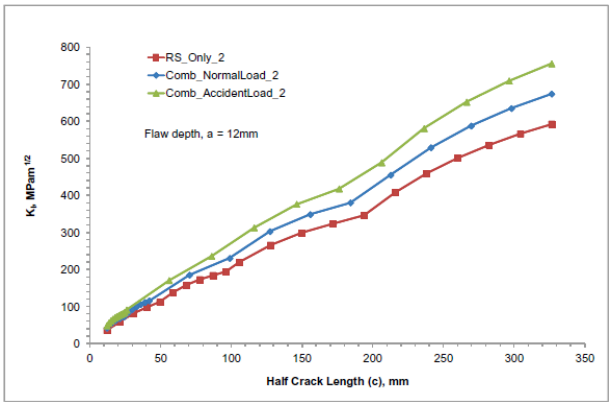

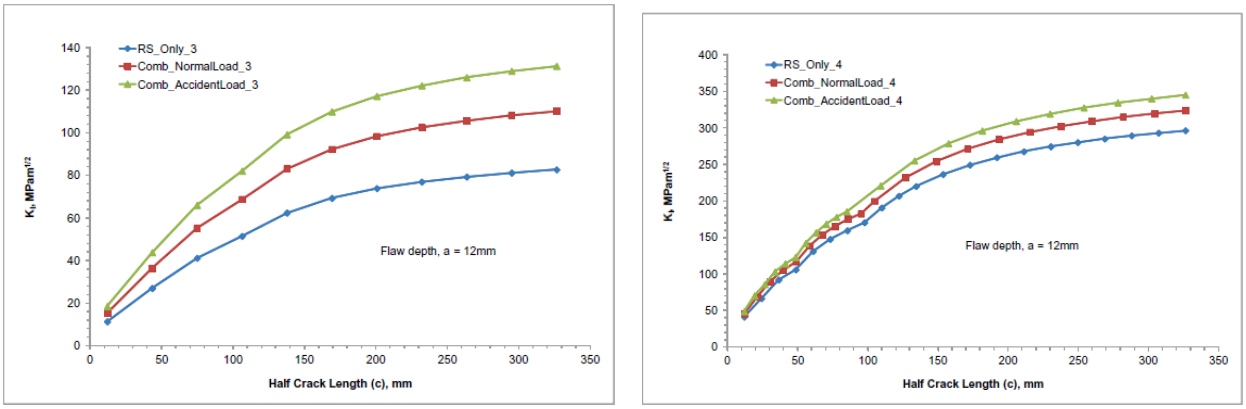

Figure 7- Welding residual stress effect on crack driving force K_I for four cases of surface cracks

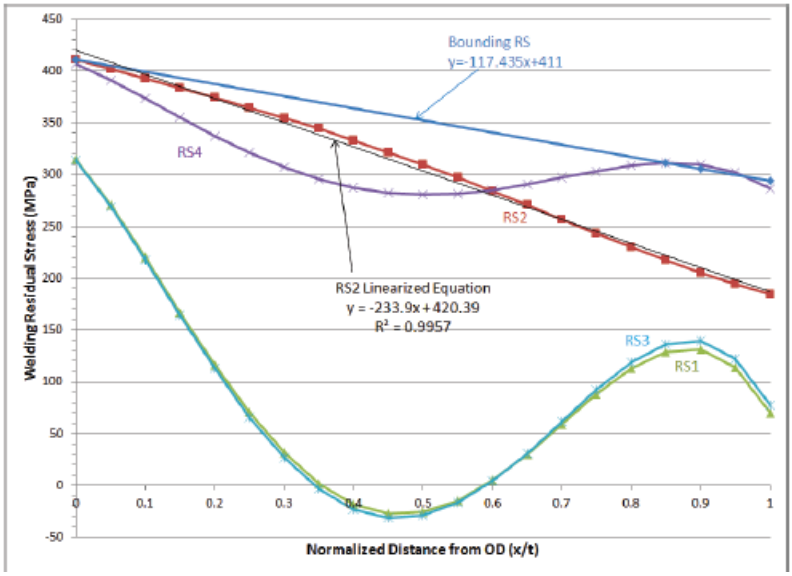

Figure 8 – Estimation of upper bounding welding residual stress

4. Residual Stress Prediction by FEA Simulations

4.1. FEA Simulation of Residual Stresses in Welded Plate

Lam et al. [18] performed an experimental and numerical study on stress corrosion cracking (SCC) of carbon steel weldments. The experiment was conducted to investigate the role of WRS on SCC in welded carbon steel plates (thickness 15.88 mm or 0.625 in.) used for nuclear waste storage tanks. Carbon steel specimen plates were butt-joined with the gas metal arc welding (GMAW) technique. Initial cracks (seed cracks) were machined across the weld and in the HAZ, as shown in Figure 9. It was observed that SCC occurred in the as-welded plate but not in the stress-relieved duplicate. A detailed FEA to simulate exactly the welding process was carried out, and the resulting temperature history was used to calculate the WRS distribution in the plate for characterizing the observed SCC. It was shown that the cracking can be predicted for the TW

cracks perpendicular to the weld by comparing the experimental K_{ISCC} to the calculated SIF due to the WRS. The predicted crack lengths agree reasonably well with the test data.

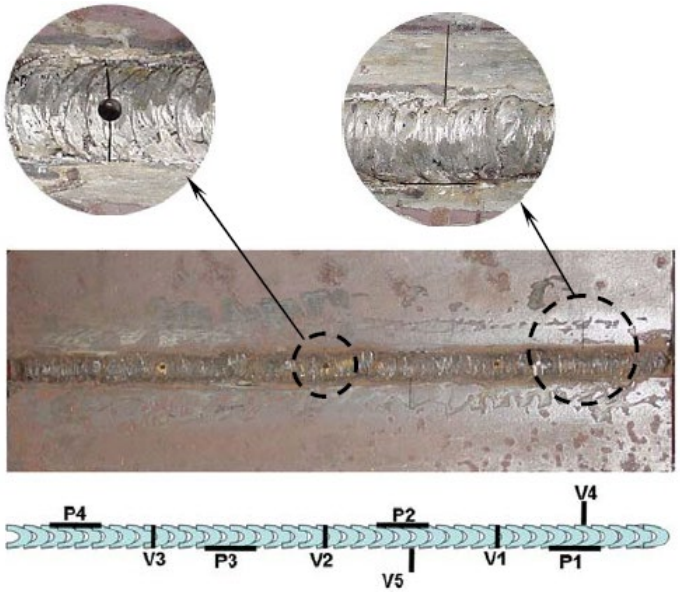

Figure 9 - Welded sample and seed crack arrangement.

Two A285 carbon steel plates were welded by gas metal arc welding (GMAW) to form a large plate. One large welded- plate was heat treated with the standard treatment for stress relief, while a second remained as-welded. Nine seed cracks were machined within the HAZ utilizing electrical discharge machining (EDM). Figure 9 shows the crack arrangement: V1, V2, and V3 are the vertical cracks across the weld through the thickness of the plate; V4 and V5 are the part-through vertical cracks; P1, P2, P3, and P4 are the part-through parallel cracks. The seed crack lengths are nominally 12.7 mm (0.5 in.), and the depth was 25% of the plate thickness (15.88 mm or 0.625 in.) for the PTW cracks.

Crack propagation of vertical crack V2. Following the ABAQUS FEA procedure, a TW vertical crack across the weld is created in an initially intact plate with as-welded RS. The crack length is incrementally increased in a self-similar manner, resulting in a continuous redistribution of the WRS. The largest stress component is found to be the longitudinal stress (σ_{xx}), and this stress component coincides with the Mode-I crack opening stress for the crack V2. The other stress components are about 10% of σ_{xx}. Therefore, crack extension is under Mode-I loading, and the SIF is K_I.

Figure 10 shows the residual stress component (σ_{xx}) for Mode-I crack extension of V2. The stress redistributions due to crack growth (for crack lengths, respectively 12 mm and 68 mm) can be compared with the that for as-welded, crack-free plate (i.e., a = 0). The stress concentration near the crack tip is clearly demonstrated in the figure. The three-dimensional (3D) FEA calculated Mode-I K factor is a function of crack extension. Using the threshold stress intensity as the metric for crack propagation, this WRS field would drive the seed crack V2 from the initial length of 12.7 mm (0.5 in.) to a final length of about 78 mm (3.1 in) at the stress intensity condition where K

equals K_{ISCC} = 35 MPa√m (32 ksi√in). This crack length prediction agrees reasonably well with the test data of the final crack length at 2.3 in.

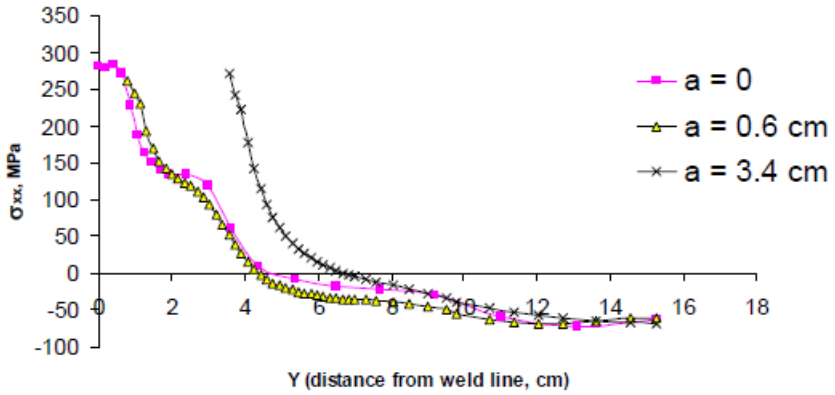

Figure 10- Distributions of the longitudinal residual stress σ_{xx} for a non-cracked welded plate (half crack length a=0) and following redistribution for two total crack lengths (12 and 68 mm).

4.2. FEA Simulation of Welding Residual Stresses in Canisters

Gim et al. [19] simulated the welding procedure for the SNF canisters to determine the WRS for both longitudinal and circumferential welding, where the welding procedure, heat analysis and stress analysis were performed, separately. The FEA results of WRS were compared with the experimental data measured by SNL [16] for a full-size mockup canister.

Figure 11 compares the FEA calculated WRS of circumferential weld with those measured WRS in its axial and hoop components. Figure 12 compares the FEA calculated WRS of longitudinal weld with those measured WRS in its axial and hoop components. From those comparisons, it is found that the FEA results of WRS are fairly consistent with the corresponding test data measured by SNL [16]. As a result, it was concluded by Gim et al. [19] that the FEA simulation seems to sufficiently confirm the experimental data of WRS.

Figure 13 shows more accurate FEA results of hoop WRS cross the wall thickness for the axial crack case obtained by Lee et al. [20] using the initial stress method.

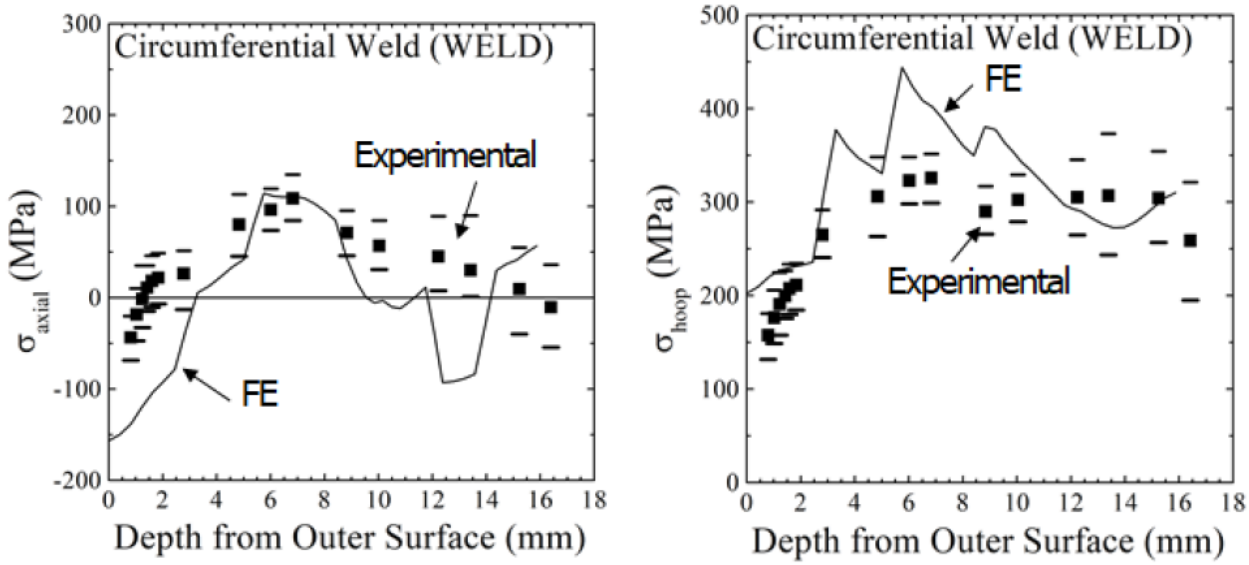

Figure 11 - WRS of circumferential weld: (a) axial stress (perpendicular to the weld) and (b) hoop stress (parallel to the weld)

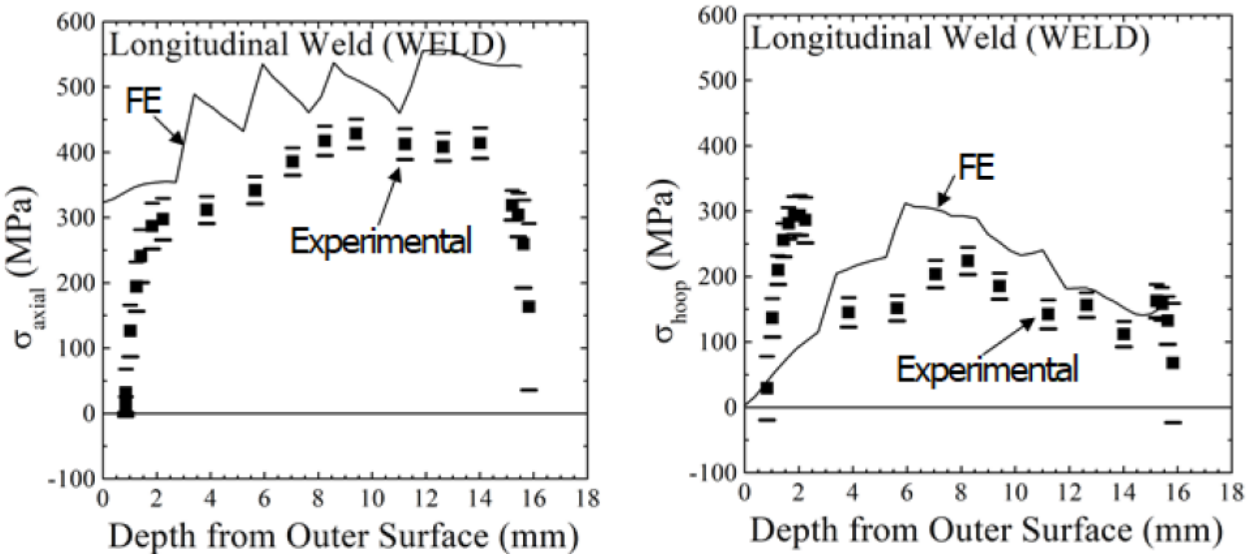

Figure 12 - WRS of longitudinal weld: (a) axial stress (parallel to the weld) and (b) hoop stress (perpendicular to the weld)

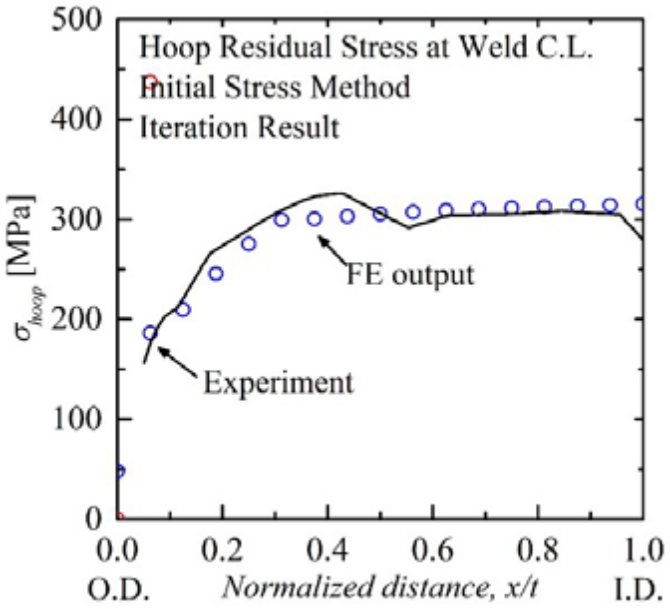

Figure 13 - Hoop WRS cross thickness at weld centerline using initial stress method

4.3. Recent FEA Simulation of Welding Residual Stresses in Canisters

Recently, Wu [21] performed 3D FEA simulations of the WRS of the welds in the mockup canister fabricated at SNL [16] and obtained accurate FEA results for WRS that match well with the DHD measured WRS. Figure 14 shows the 3D FEA model for the mockup canister with fine meshes near the welds. Figure 15 shows the temperature contours for an individual weld pass in the longitudinal welds from the FEA thermal simulation. Figure 16 shows the WRS profiles as a function of depth in (a) weld center line (WCL) and (b) HAZ of circumferential weld from the FEA mechanical simulation, where the DHD measurements of WRS are included. Each FEA result is averaged from ten points in the steady state location. The FEA results and DHD measurements of WRS agree fairly well.

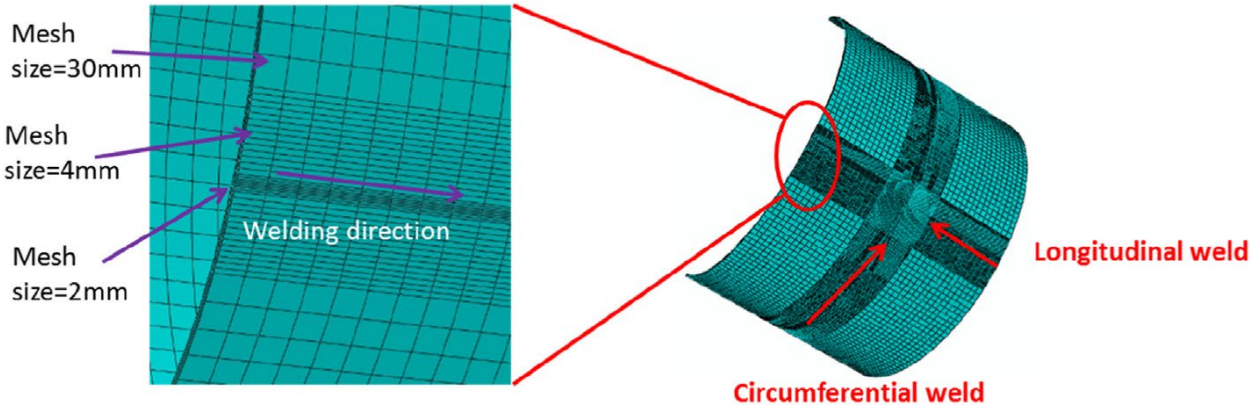

Figure 14 - The FEA model for the mockup with fine meshes near welds [21]

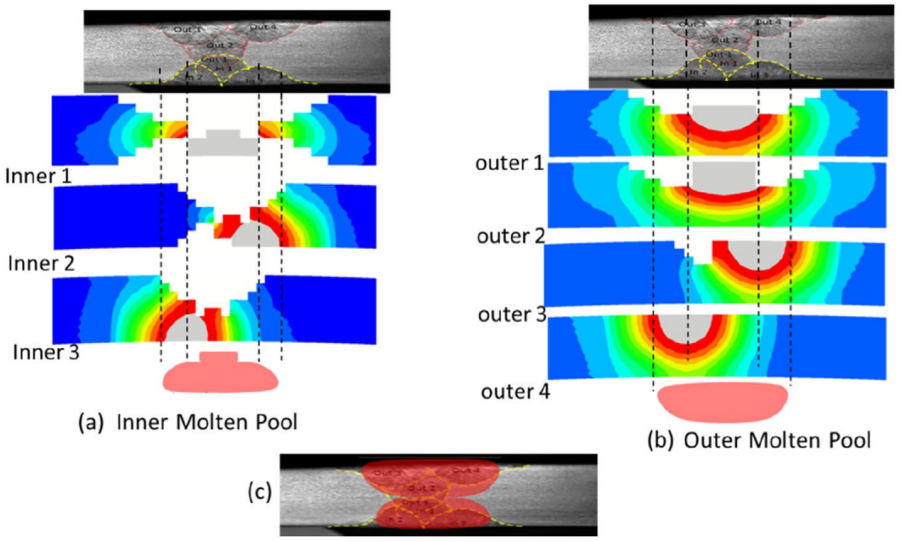

Figure 15 - Temperature contours of individual weld pass in the axial welds [21].

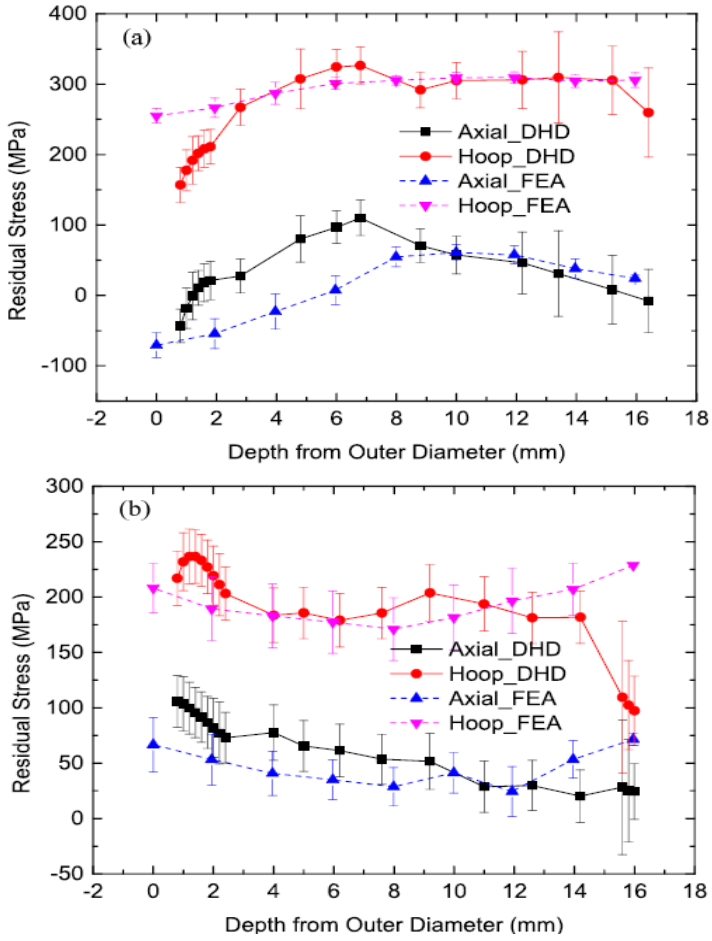

Figure 16 - Residual stress profiles as a function of depth in (a) WCL and (b) HAZ of hoop weld [21].

5. Experimental Measurements of Residual Stresses in Canister

5.1. Residual Stress Measurements at SNL

Sandia National Laboratories [SNL] fabricated a mockup canister following the standard welding procedure used in the manufacture of the standard canisters. Then they conducted the WRS measurements on the welds of the mockup canister using the traditional Deep-Hole Drilling [DHD] and incremental Deep-Hole-Drilling [iDHD] methods. They also utilized the contour method to determine a stress map over the entire cross section [16]. Figure 17 represents the hoop stress in the axial cross section of the canister containing a weld, that is, the stress contour illustrates the WRS parallel to a circumferential weld (i.e., RS 2). Figure 18 shows the axial stress in a cross section containing a longitudinal weld and the WRS is parallel to the weld direction (i.e., RS 4). These actual measurements of WRS are consistent with those estimated by Lam and Sindelar [5] in the guideline of API 579 Annex E [10]. Figure 19 shows the WRS distributions through the thickness for the weld-center line and HAZ. It clearly indicates that the WRS at the weld center line is higher than WRS at HAZ.

Figure 20 compares the measured WRS distributions cross the wall thickness with those estimated by R6 and ASME BPVC Section XI. It is shown that the measured WRS results do not agree well with the WRS distributions estimated by these codes. The root cause for the discrepancy is that the canisters have a large R/t ratio ranging from 50 to 70 (or D/t = 100 to 140), but these FFS codes cannot be used for this large range of R/t ratios.

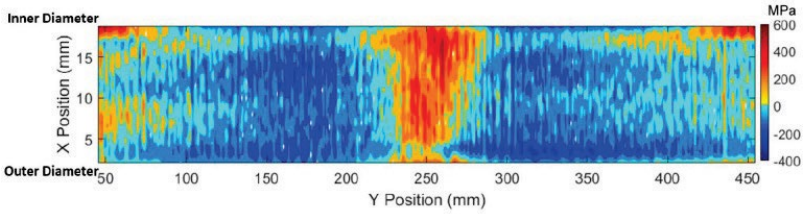

Figure 17 - Residual stress contour map parallel to a circumferential weld through the wall thickness of Sandia mockup canister [16].

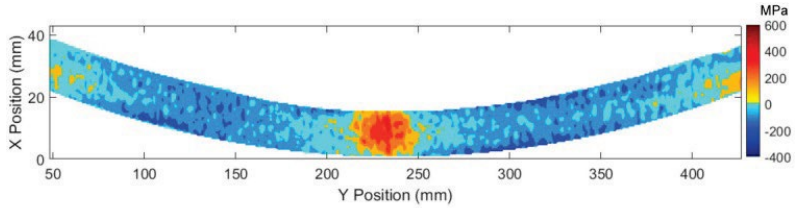

Figure 18 – Residual stress contour map parallel to a longitudinal weld through the wall thickness of Sandia mockup canister [16].

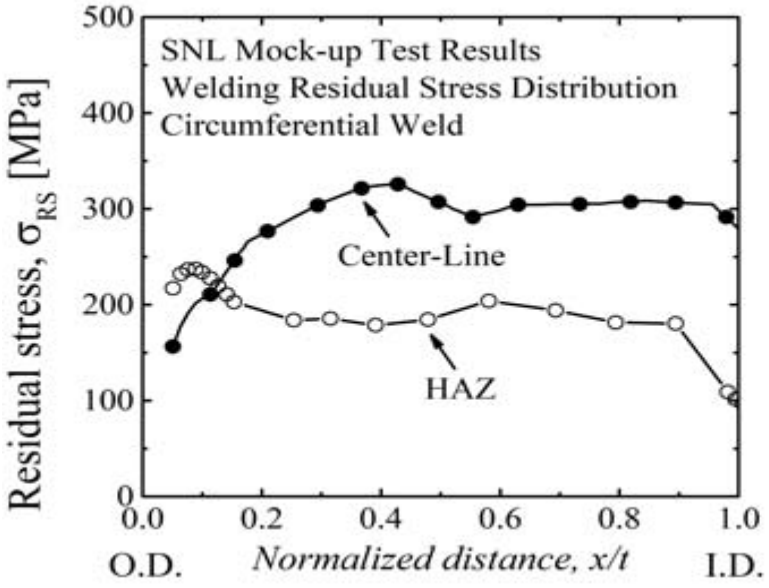

Figure 19 – Sandia mockup test results of hoop WRS distribution along thickness at circumferential weld center line and HAZ [16].

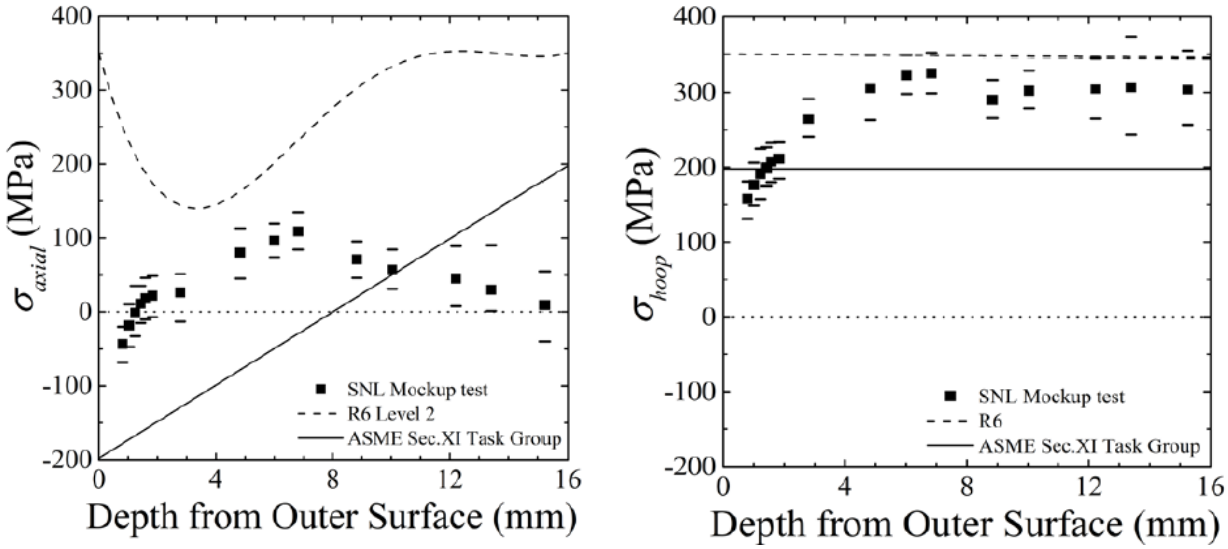

Figure 20 - Comparison of measured hoop and axial WRS with Code estimations [5].

5.2. Residual Stress Analysis at SRNL

Duncan et al. [22] and Lam et al. [23] recently conducted a CISCC experiment driven by WRS using a large plate as the test specimen. The large plate of 51 x 46 cm with a thickness of 16 mm that contains an as-fabricated circumferential weld was cut from a full-scale mockup SNF canister [16]. The mockup canister has an OD of 1.7 m (67.25 in.) and WT of 15.875 mm (0.625 in.), leading to D/t=106.6. Three 1.2 m (48 in.) cylindrical shell sections were circumferentially welded, and the big plate with a weight of 30 kg was cut from one of the two circumferential welds in the mockup canister. A set of PTW and TW seed cracks were machined by EDM wires (0.25 mm diameter) in the WRS region. The K factors were calculated by following the API 579 procedures

to provide insight into crack initiation and growth under WRS. The size of the sectioned plate was carefully determined from a series of FEA calculations to minimize the redistribution or relieving to WRS due to cutting. Thus, it is reasonable to assume that the RS in the large plate would be similar to those reported in the experiment by Enos and Bryan [16].

Figure 21 illustrates the seven seed cracks machined into the large plate with the circumferential weld. They were intended to create a favorable fracture environment for a SCC to initiate and grow under the WRS loading. The seed crack tips are located in the weld and the HAZ region. The seven crack designations are:

(a) VT1, VT2: TW crack across the weld, crack length = 25 mm.
(b) HT1: TW crack parallel to the weld edge, crack length = 12 mm.
(c) VP1, VP2, VP3: semi-circular PTW crack perpendicular to the weld edge, crack length = 12 mm and crack depth = 6 mm.
(d) HP1: semi-circular PTW crack parallel to the weld edge, crack length = 12 mm and crack depth = 6 mm.

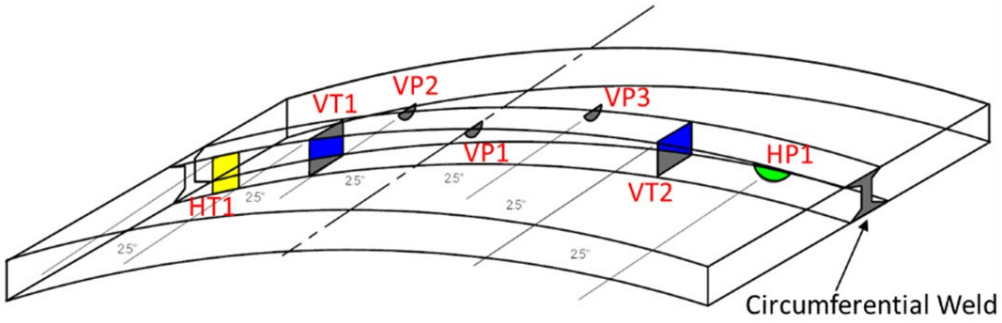

Figure 21 - EDM starter cracks schematics along the circumferential weld [23].

Artificial sea salt was prepared by following the procedure recommended in ASTM D1141, and then deposited on the OD surface of the plate with an air brush. The intention was to increase the likelihood of SCC occurrence. To provide an insight for the tendency for crack propagation, the K factors were calculated for the cracks. Korean University (KU), under the I-NERI [24] joint project, adopted the API 579 procedures to obtain the K factor solutions. Both WRS measured at the WCL and HAZ were considered in the calculation. The WRS and its curve-fitting coefficients are given in Figures 22-25.

With these WRS distributions cross the wall thickness, the K factors were calculated for all seven machined cracks following the API 579 procedure, as shown in Figure 26. The KU laboratory tests in 5% salinity artificial seawater at room temperature 50 ^{o}C showed that the threshold of SIF was about 15 MPa$\sqrt{m}$ for the canister. Therefore, based on the calculated results of the K factors, as shown in Figure 26, CISCC could occur in the large plate, especially for the machined cracks perpendicular to the weld, as shown in Figure 26, if the as-fabricated WRS was not significantly altered or relieved by the plate sectioning from the mockup canister and by EDM machining for starter cracks.

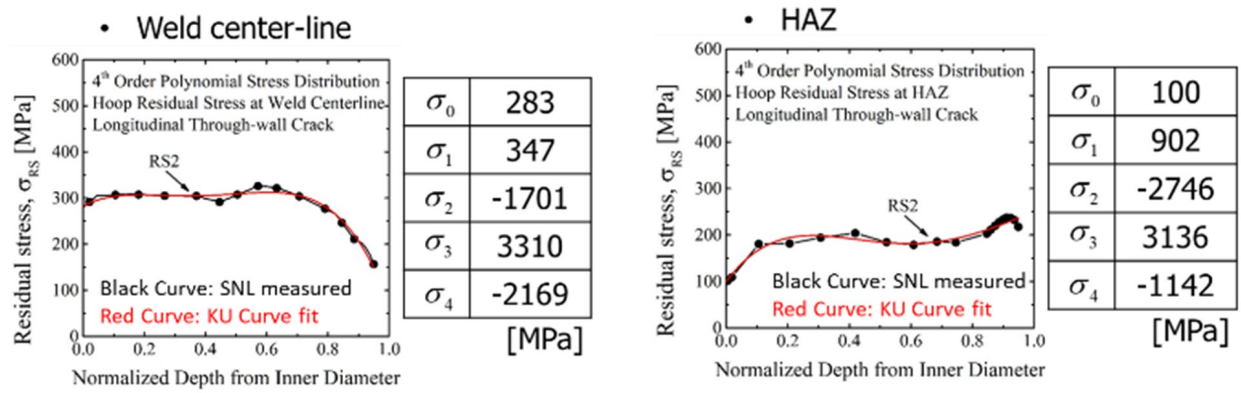

Figure 22 - Welding residual stress parallel to the circumferential weld: RS2, x=0 at ID

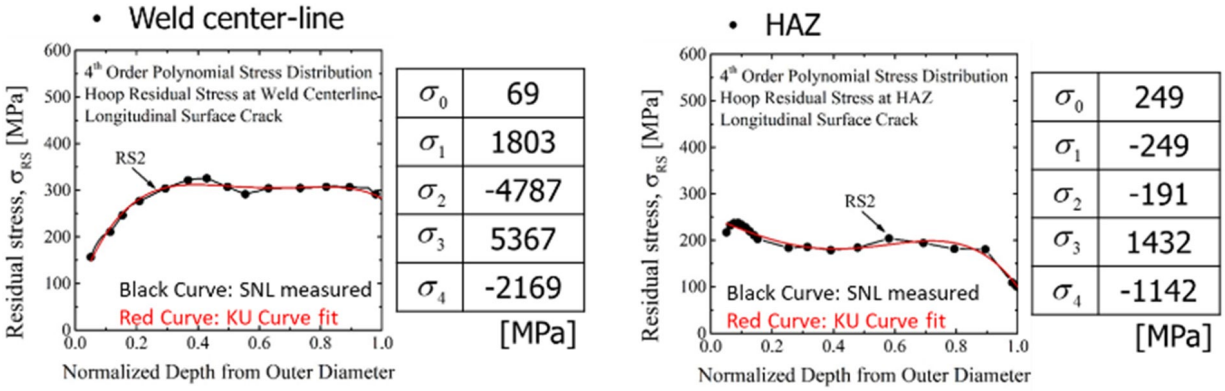

Figure 23 - Welding residual stress parallel to the circumferential weld: RS2, x=0 at OD

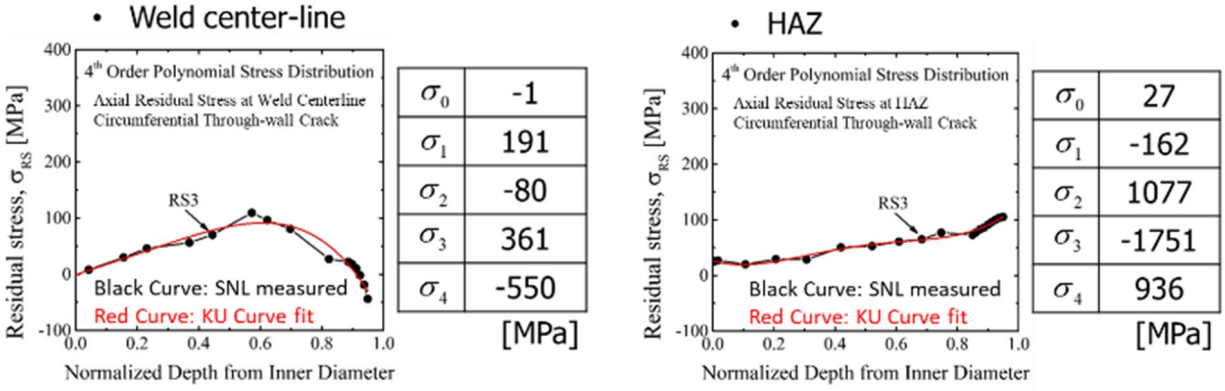

Figure 24 - Welding residual stress perpendicular to the circumferential weld: RS3, x=0 at ID

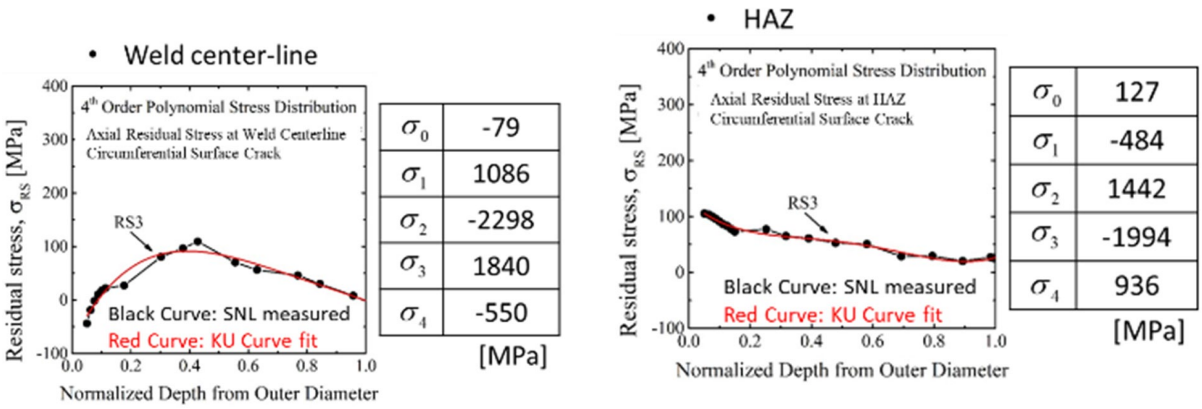

Figure 25 - Welding residual stress perpendicular to the circumferential weld: RS3, x=0 at OD

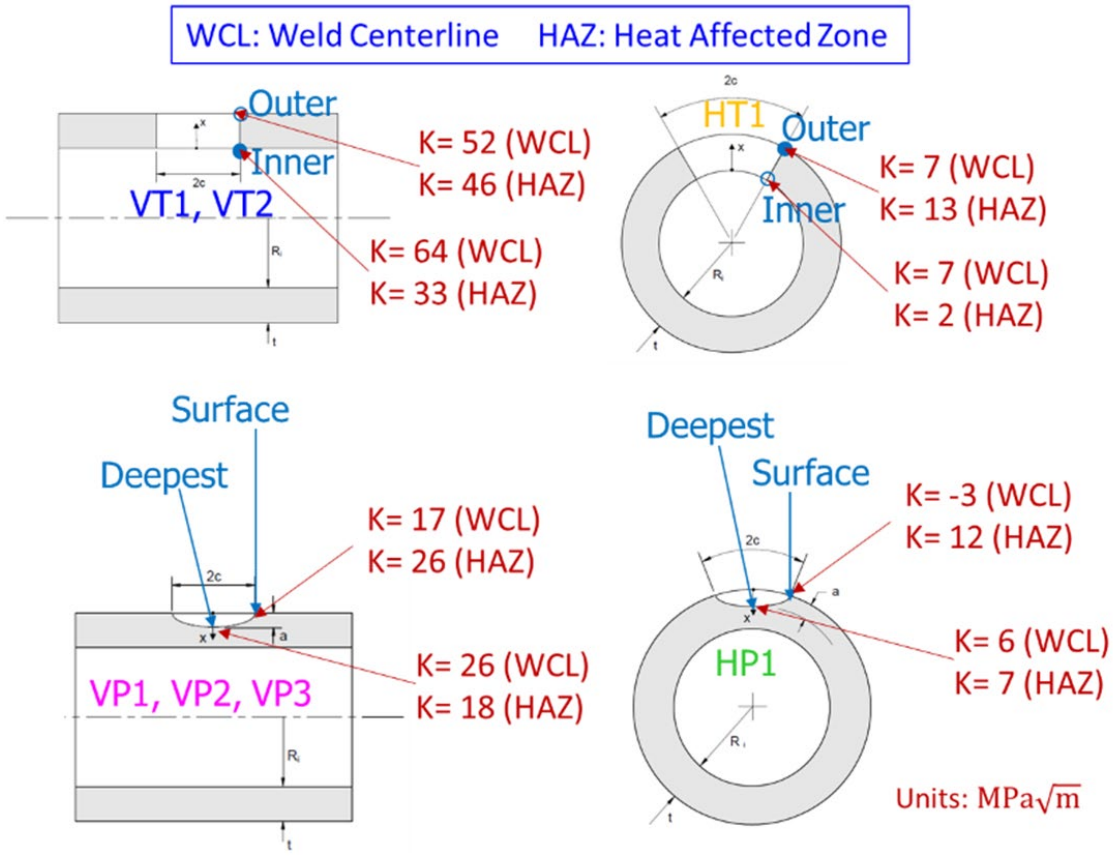

Figure 26 - Stress intensity factor results for the seven machined cracks

6. Residual Stresses in Canisters after Post-Weld Treatment

As noted, the canisters are not required to be PWHT after welding so that WRS remain from fabrication. To mitigate the tensile WRS, some other post-weld treatments, such as cold spray and laser peening, have been investigated.

6.1. Residual stresses in restrained plates after cold spray at EPRI and PNNL

Recently, Electric Power Research Institute (EPRI) [25] and Pacific Northwest National Laboratory (PNNL) [26] performed the WRS analysis of cold spray deposition for SCC mitigation and repair. Cold spray technology is a solid-state power deposition process that is considered a top candidate for in-service canister mitigation and repair. This process is a variant of thermal spray and applies the powder materials at supersonic speeds to produce a combined mechanical and metallurgical bond with the metallic substrate, as shown in Figure 27.

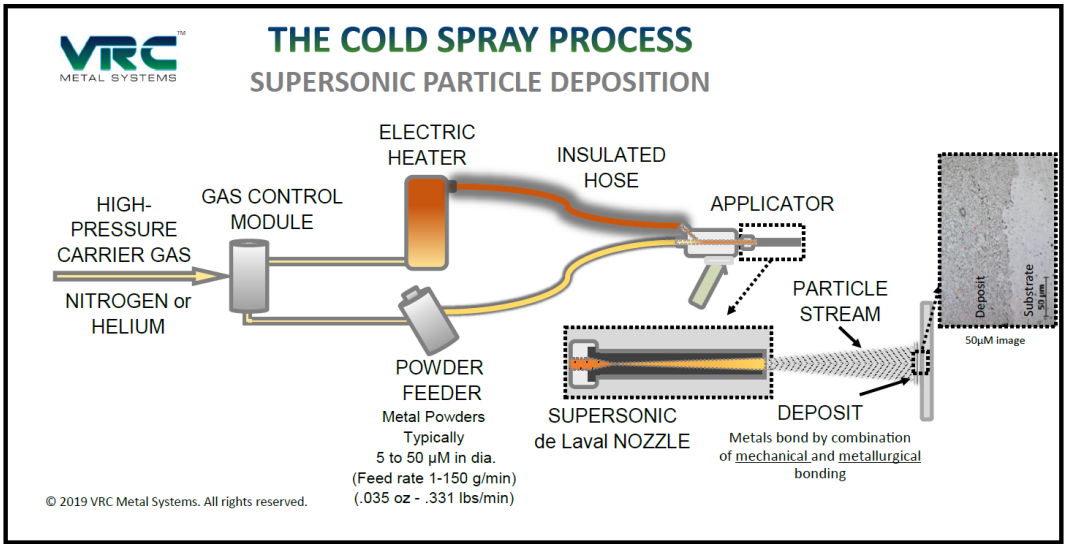

Figure 27 - Schematic of the cold spray process [25]

One notable advantage of the cold spray process is that the melting point temperatures are not reached during powder deposition in comparison with the thermal spray with the highest temperature at the metal melting point. Cold spray used for canister mitigation and repair can reduce the WRS on surface in the deposition region on the welds. Therefore, Tatman [25] performed an extensive analysis on conservatively designed mockups to quantify the anticipated magnitude of RS reduction when applying cold spray deposits on canister welds.

Two identical weld mockups were fabricated to simulate the longitudinal seam welds performed on canisters in Dry Cask Storage System (DCSS). Each mockup consisted of two 0.5-in (12.7 mm) thick AISI 304/304L SS plates and were welded using AISI 308/308L filler material. The joint configuration consisted of a single V-groove geometry and was welded using a multi-pass high heat input GTAW procedure. To provide representative restraint conditions on the plates to be

welded, the plates were bolted to a thick section backing plate of low alloy steel. Figure 28 shows a completed weld assembly in the restrained and bolted conditions.

Figure 28 - Completed weld assembly in the bolted and restrained condition [25]

One of the two fabricated high restraint weld mockups had cold spray deposition in the designated region of one half of the weldment [25]. The following information was provided on the test deposits by cold spray:

- The substrate material was 0.25-in. thick 304 stainless steel.
- Helium was the driver gas used for the test sprays.
- The deposit material was Inconel 625 powder.
- Coupons were sprayed for each booth qualification and bookend and contained with minimum dimensions of 1 in. x 4 in.
- Adhesion tests were performed on each coupon with a portable adhesion tester.
- Porosity was examined in multiple locations and calculated per ASTM E1382-97 (2015).

Following acceptable evaluation of the test setup and parameters, in a selected region having 8-in (203 mm) in length by 5-in (127 mm) in width by 0.04-in (1 mm) in depth, Inconel 625 buildup was deposited on the high restraint weld mockup, as shown in Figure 29. It is seen that the selected region for cold spray covers about one half of the weldment. After the cold spray was completed, the residual stress analysis was performed by EPRI (contracted Hill Engineering) using the incremental hole drilling technique for the cold sprayed weld mockup [25].

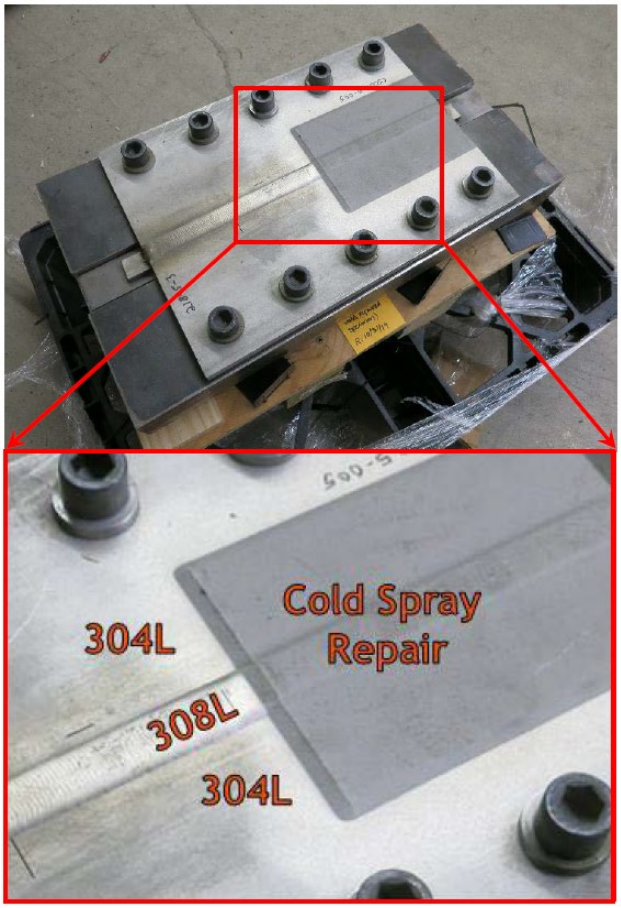

Figure 29 - Inconel 625 cold spray buildup deposited on high restraint weld mockup [25]

Hole drilling measurements were performed within the cold spray (CS) buildup to evaluate the magnitude of longitudinal (x-axis) and transverse (y-axis) WRS reduction in the weld zone (HD1 and HD13), HAZ (HD2, HD3, HD12, HD14), and base metal (HD4, HD5, HD11, HD15) regions of the as-welded (AW) mockup [25]. Note that the designations HD1 to HD15 were defined to represent different locations where a hole was drilled. Duplicate measurements were performed at the same locations on the as-welded (AW) high restraint mockup to determine the difference from the CS deposition. Figures 30, 31, and 32 display the results of these WRS measurements. From these figures, the observations are made:

- All measurements on the CS buildup were compressive and revealed a substantial decrease in plate WRS when compared to the AW condition. The average and max decrease of RS was in HAZ.
- Weld HAZ on canisters has the greatest propensity, and so stress minimization is most critical in this region. The highly compressive measurements show the CS process may be an effective method for RS reduction in the HAZ.
- The smallest decrease in RS from CS deposition was in the base metal region.

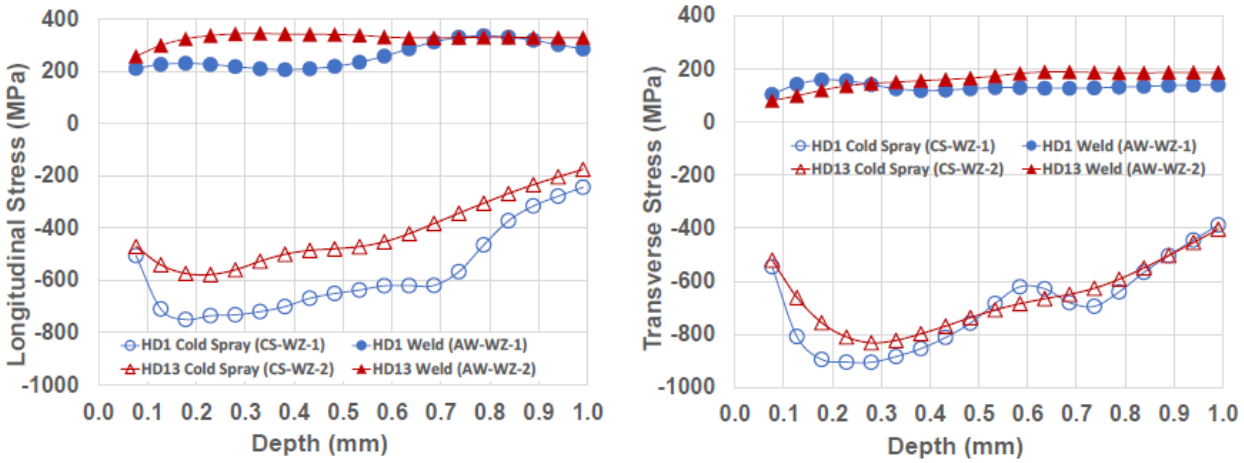

Figure 30 - HD1 and HD13 measured results of longitudinal and transverse WRS at the weld centerline of CS and AW mockups [25]

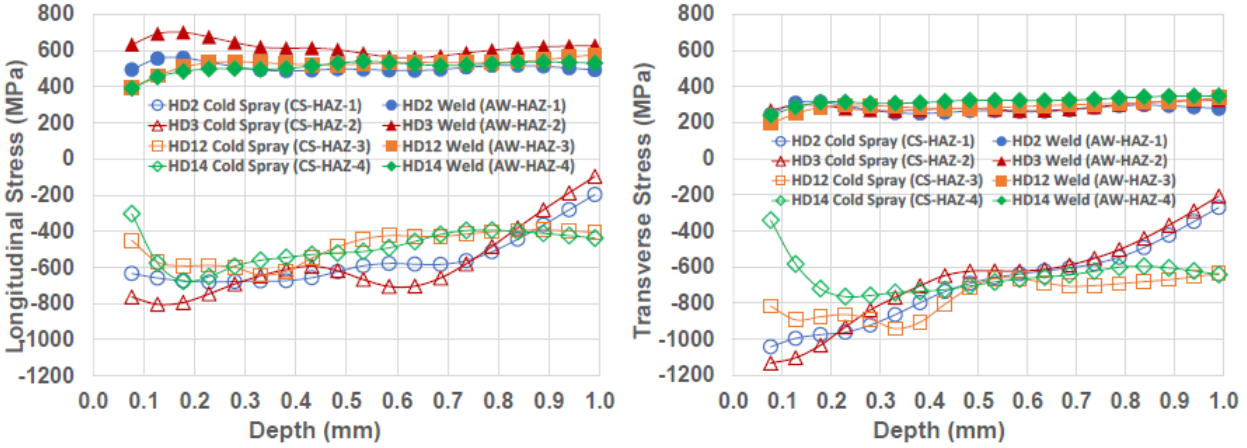

Figure 31 – HD2, HD3, HD12 and HD14 measured results of longitudinal and transverse WRS in the HAZ region of CS and AW mockups [25]

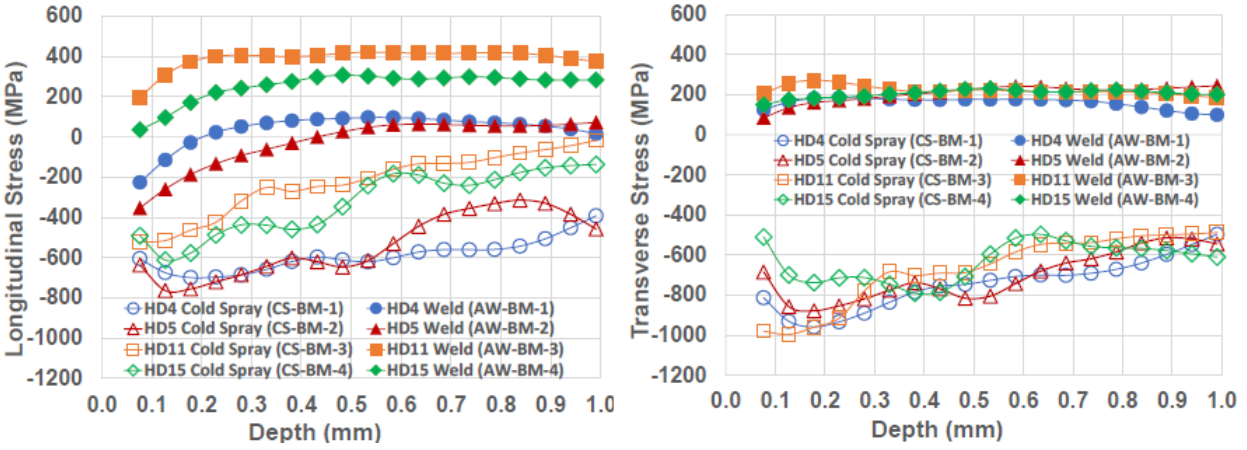

Figure 32 – HD4, HD5, HD11 and HD15 measured results of longitudinal and transverse WRS in the base metal region of CS and AW mockups [25]

6.2. **Residual stress reduction in mockup canister after laser peening**

Laser peening [27] can provide a compressive stress deeper than minimally required and a technology that can be efficiently applied to large structures with high reliability.

Laser peening [27] has been demonstrated to effect compressive stresses at depths greater than 5 mm. The test program performed by Hackel et. al. [27] centered on using relatively large (11 in. x 11in.) panels of 316L steel of thickness 0.65 in. for peening and WRS measurements and using relatively smaller (6 x 5 x 0.65 in.) panels for CISCC testing. Panels were laser peened over one half of their area with the other half left in an unpeened as welded state enabling simultaneous exposure and testing of the peened vs unpeened area. The WRS was measured by the Hill Engineering using the contour method.

Peening is a process that plastically compresses surface material resulting in transverse (Poisson's) expansion. Other compressive surface treatments include short, laser, and ultrasonic peening. Among them, laser peening employs high pressure plasma that generates fully normal compressive force. Figure 33 illustrates the laser peening process. At nanosecond scale, intense laser pulses create a plasma in a confined geometry and thus generate pressure pulses sufficiently intense to plastically deform the local surface adjacent to the weld being treated. In general, hardness and yield strength of the treated material remain nearly unchanged. Higher energy laser peening employs laser energy output in the range of 20 J/pulse that enables the use of a relatively large area (1 cm^2) so that the shock wave can penetrate deep beneath the surface as a planar wave before geometrically rarefying to generate a deep compressive stress.

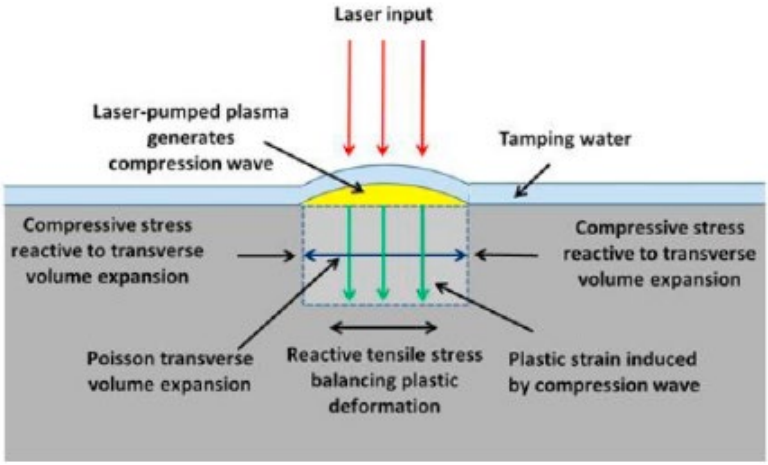

Figure 33 - Illustration of laser peening that plastically compresses material normal to a surface generating a transverse compressive stress [27]

Figure 34 shows an example of the deep compressive stress generated by high-energy laser peening performed on 316L SS. WRS measurements were made using a slitting technique. In this figure, the dark diamonds represent the computed WRS as a function of depth in the test block; the linear dashed line is a fit to the slope of the bending stress profile resulting from the bending the panel; and the open markers represent the summation of measured stress and resultant bending stress. The latter stress is also known as the equivalent stress or eigenstress that would have resulted from an infinitely thick panel. This represents the actual depth of plastic response to the

laser peening. From the data in Figure 34, it can be concluded that the plastic deformation of the laser peening penetrated to approximately 11 mm. It is critical that the pitting depth does not reach a tensile layer under the peening compressive laser, as shown in Figure 35. Laser peening provides a very robust safety factor such that the compressive stress layer depth extends several times deeper than the potential pit growth depth.

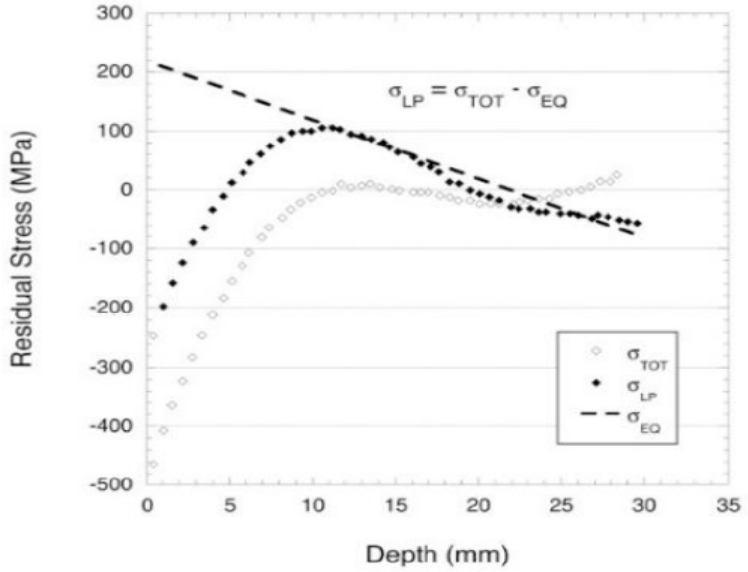

Figure 34 - Residual stress measured in 316L SS that was laser peened at 8 GW/cm² irradiance [27]

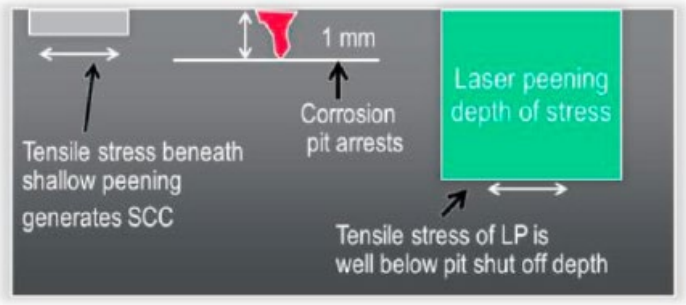

Figure 35 – Illustration of tensile stress beneath shallow peening [27]

Figure 36 shows a test panel that was roll-formed and welded per the SNF canister fabrication procedures. The weld runs from left to right. WRSs were measured by the contour technique on the free-edge coupon after laser peening and calculated using the FEA simulations, where the canister FEA model was calibrated from the panel measured results. Canister panel virtually peened and stress calculated in a panel section of a canister. Reduced stress in free panel was calculated and compared to that measured in the welds of the canister. Figure 37 shows an example

calculation where the stress retained in the canister is 5.5 mm and approximately 2 mm deeper than that measured in the panel.

Figure 36 – Welded test panel using the canister welding procedure: top view and side view [27]

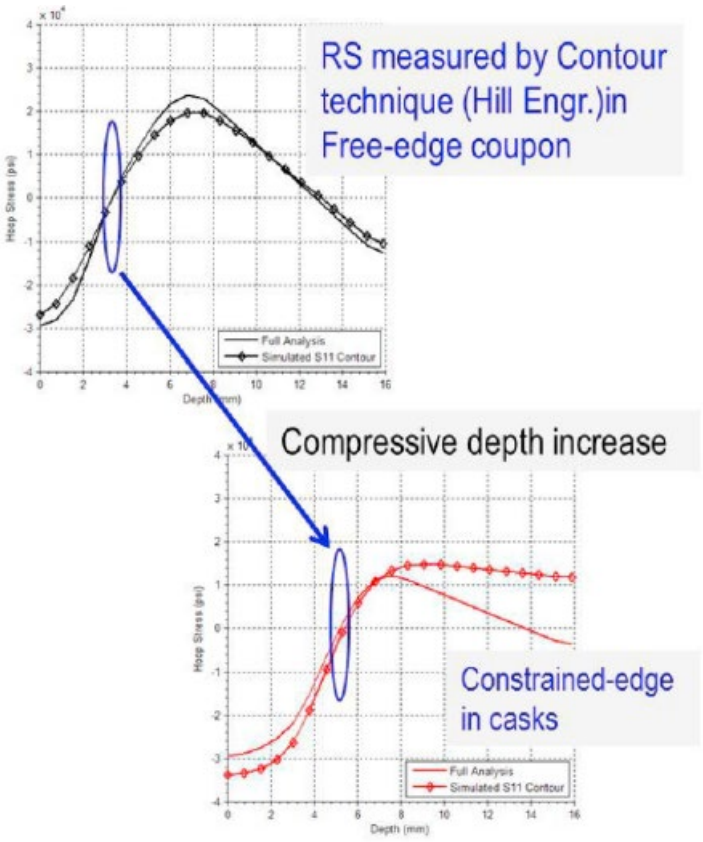

Figure 37 - Comparison of FEA and measured hoop WRS in the test panel and in a canister [27]

6.3. Residual stress reduction in welded pipeline after local post-weld heat treatment

A weld joint consists of three metallurgically different regions: weld metal, HAZ, and base metal. The WRS are introduced during welding as a result of base metal restraint of the shrinkage of hot weld metal during cooling. Multi-pass narrow gas welding requires lower heat input during welding that also introduces lower levels of WRS. Post Weld Heat Treatment (PWHT) is applied

after welding to reduce the WRS in thick-wall components. It is an optional procedure in fabrication practice. Standard PWHT is conducted in an enclosed furnace for a few hours to remove the hydrogen, improve fracture toughness and relieve WRS in components. However, in the circumstances that conventional furnace PWHT is not feasible due to large sizes like the SNF canisters, local PWHT [28] may be considered as an alternative. In terms of relief of WRS, the PWHT holding temperature has been demonstrated to be more critical than the holding time, as specified in BS 7910. An example of the use of local PWHT for relieving WRS is given below.

A girth weld was fabricated by joining two X65 pipes. Each pipe has a length of 750 mm (29.5 in.), an OD of 355.6 mm (14 in.) and a WT of 19.05 mm (0.75 in.), leading to D/t = 18 for a thick-wall pipe. Six passes of the filler metal were deposited into the weld groove, and the weld was fabricated by the pulsed GMAW process. The WRS was measured using the neutron diffraction (ND) technology. The principles of ND are based on the Bragg's and Hooke's Laws. In a polycrystalline material, only the grain lattice planes, which allow Bragg reflection and contribute to the scattering.

In order to investigate the effectiveness of PWHT on the relief of WRS, the WRS was measured in the As-Welded (AW) condition. One pipe spool ($P_{HT}1$) was locally heat treated by using an electrical resistance heating blanket for a period of 1 hour. Another pipe spool ($P_{HT}2$) went through the conventional furnace heat treatment for the same length of time. Figure 38 shows a general sketch of the local circumferential PWHT parameters as well as their terminologies.

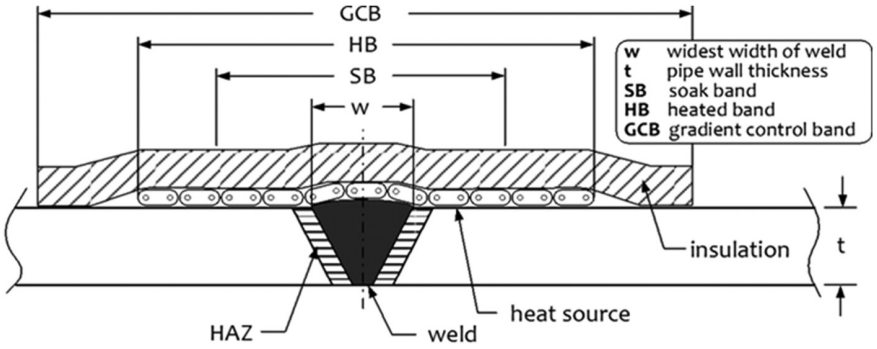

Figure 38 - Sketch of the parameters for local circumferential PWHT [28].

The WRS were measured for the three conditions of AW ($P_{AW}1$ and $P_{AW}2$), local PWTH ($P_{HT}1$), and furnace PWHT ($P_{HT}2$). Figure 39 compares the through-thickness RS at the weld center and the toe before and after local and furnace PWHT for the hoop and axial directions, respectively, together with the profiles estimated from R6 and BS 7910. In the figures, the longitudinal RS were normalized using the greater yield strength σ^{+}_{y} of the weld and base metals, and the transverse RS were normalized using the smaller yield strength σ^{*}_{y} of the weld and base metals.

Figure 39(a) shows that the through-thickness hoop WRS at the weld center of two pipes display overall similar trends to BS 7910 and R6 Level 2 profiles. Figure 39(b) shows that axial WRS near the pipe OD surface are tensile and balanced by compressive RS near the ID surface. The highest axial RS is 40% of the room temperature yield strength of the base metal. Similar though-thickness

WRS distribution and magnitude are found at the weld toe. In general, WRS profiles obtained from measurements are below the upper bounds advised in the codes and standards. It is concluded that the local PWHT can achieve the same magnitude of WRS relief as the global PWHT.

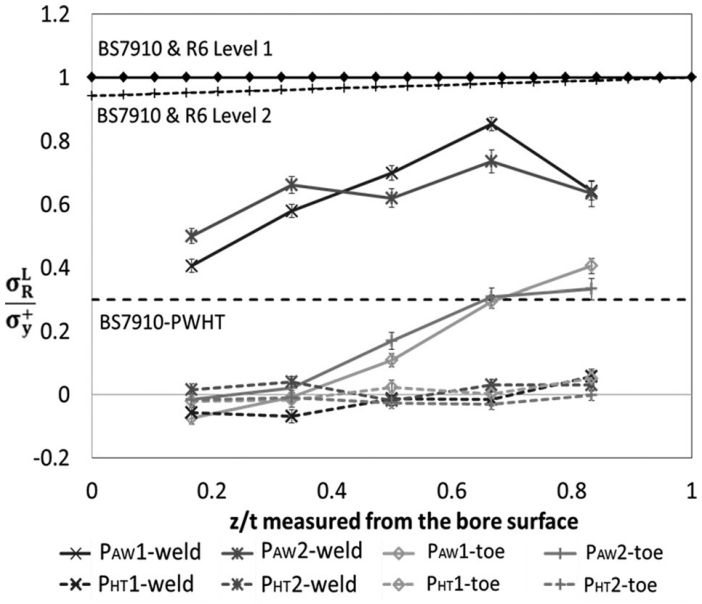

(*a*)

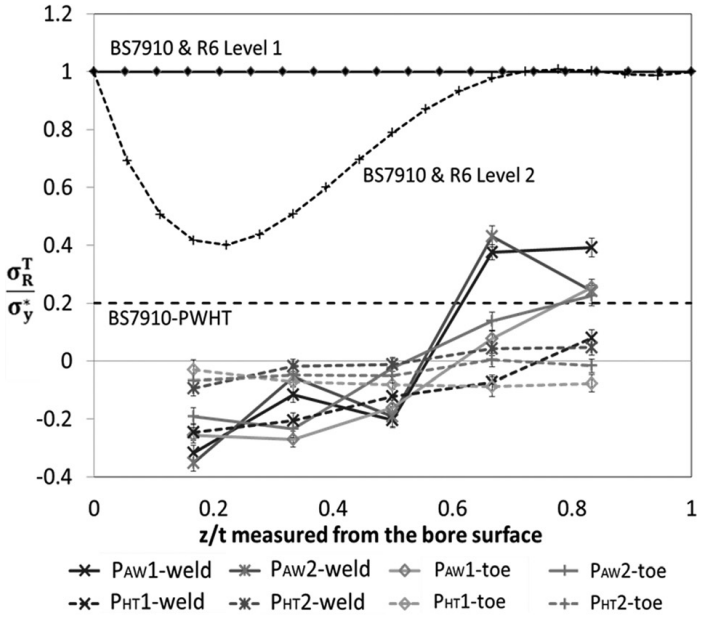

(*b*)

Figure 39 – comparison of the through-thickness residual stresses at weld center, and weld toe before and after local and furnace PWHT with those from R6 and BS 7910.

7. Residual Stresses in Spent Canisters after Fusion Welding Repair

In order to reduce WRS generated in the weld fusion zone (FZ) and HAZ of welded joints in SNF canisters, Oak Ridge National Laboratory [29, 30, 31] investigated traditional fusion welding

technology to repair the cracks in the original welds. The as-welded specimens were provided by SNL [16] from a canister mockup manufactured using procedures similar to those used for actual canister production. ASME-qualified GTAW was used to repair the AW specimens, and post-repair WRS were measured using neutron diffraction (ND) technology. AW and repaired specimen RS distributions were evaluated and compared. Significant RS profiles were identified from the received AW longitudinal weld sample. The generated RS profile from the ND was similar to that of SNL WRS data obtained from the DHD technology. The GTAW-repaired specimen showed a notable redistribution in RS and even introduced compressive stresses when compared with the AW condition. It appears that groove excavation and the well-controlled GTAW heat input effected low residual stress.

WRS is generated in metal structures as a result of irregular elastic-plastic deformation during welding. The WRS distribution can be measured by destructive or nondestructive methods. Destructive methods include shallow and deep hole drilling that typically provide localized carriable depth measurements. Nondestructive methods include X-ray or neutron diffraction. Due to sample thickness, X-ray diffraction can only penetrate a few μm. Thus, neutron diffraction was selected by ORNL as it is the only technique that can provide a 3D mapping of RS without damaging the welded sample, as shown in Figure 40.

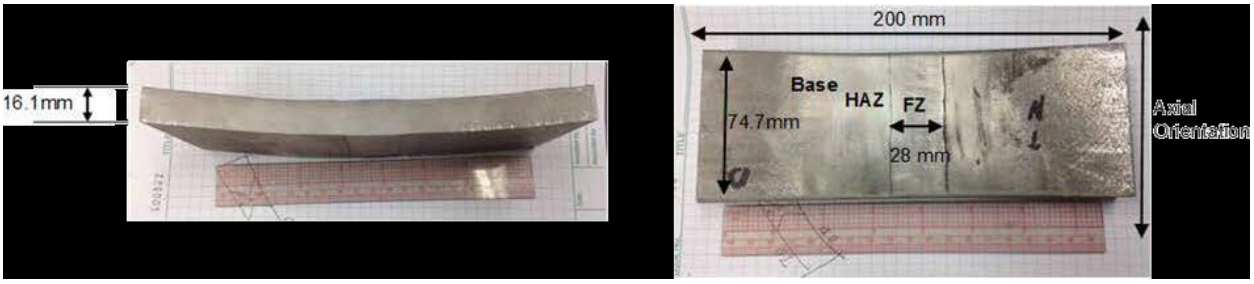

Figure 40 - The received weld plate sectioned from SNL full-scale mockup SNF canister [29]

The received AW specimen was first measured on WRS by neutron diffraction. Next, a groove was excavated using EDM to simulate crack removal and the weld metal was deposited using GTAW to simulate a remote repair, as shown in Figure 41. The repaired and original welding microstructures of the specimen is shown in Figure 42.

Then the WRS on the repaired specimen was measured again by the neutron diffraction. Residual strains in the x (hoop), y (radial), and z (axial) directions along five selected contours were measured. The measured strains in the radial direction were near zero. The details of the test results for the hoop and axial RS profiles for as-welded and repaired specimens are shown in Figures 43-46, respectively. It is recognized that constraint of the plate during welding (vis-à-vis an unconstrained plate) would likely increase RS and thus weld-specific conditions need to be well-characterized.

Figure 41 - The welded specimen: (a) Groove excavation and (b) GTAW repaired specimen [29]

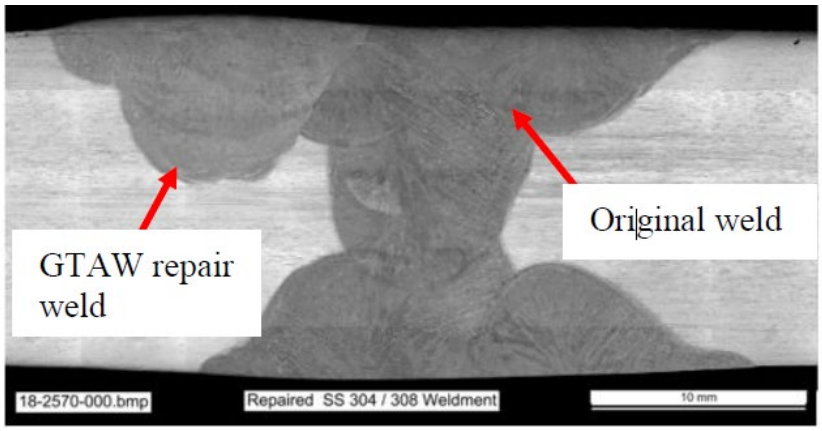

Figure 42 - Micrograph of specimen with repaired and original welding microstructures [29]

From Figures 43-46, it is observed that the maximum tensile WRS for the AW specimen is 340 MPa, and the maximum WRS is located in fusion zone (FZ) and oriented in the axial direction that is much higher than the yield stress of 200 MPa for the 304L steel. It also indicates that tensile WRS exists throughout the thickness of the weldment in the FZ. The maximum hoop tensile WRS has a value of 283 MPa and is located in the FZ near the OD surface. It also indicates that tensile stresses exist throughout the thickness of the weldment in the FZ. Comparisons show that the WRS profiles estimated from ORNL neutron diffraction measurements and SNL DHD measurements are in good agreement, although there are differences in profile shape. This may be attributed to the fact that the received weldment sample was cut from the parent mockup canister, and a significant redistribution and relaxation of RS may have occurred during the cutting process.

For the repaired specimen, the maximum axial tensile WRS has been increased by about 65 MP to 406 MPa from 340 MPa on the AW specimen, and there is a shift in position. However, the full profile in not tensile through thickness, and there are regions where compressive stresses have been introduced. Similarly, for the repaired hoop WRS has been significantly reduced as compared with the as-welded RS. This indicates that the repair could redistribute the stresses in a beneficial way.

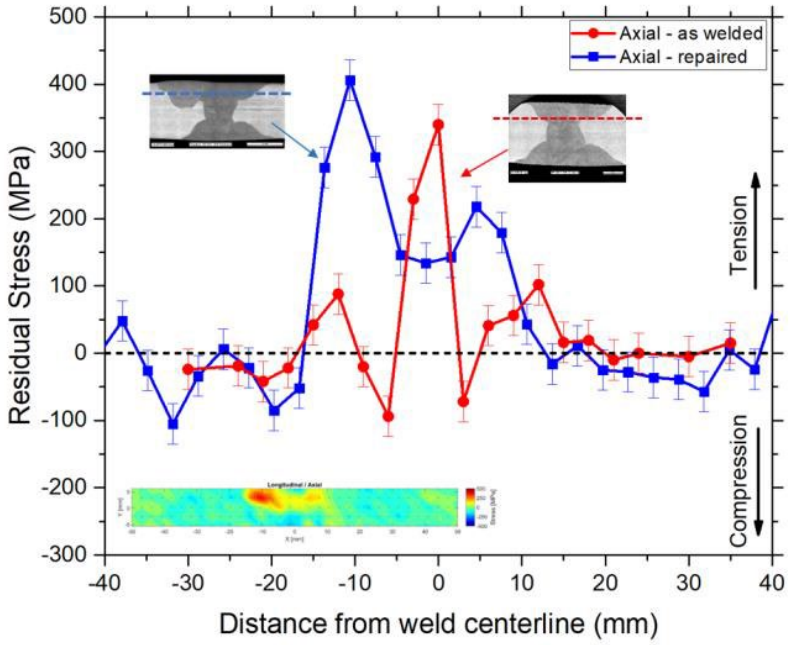

Figure 43 – Axial WRS profiles perpendicular to the weld as AW and repaired specimens at the location of 3.3 mm from OD.

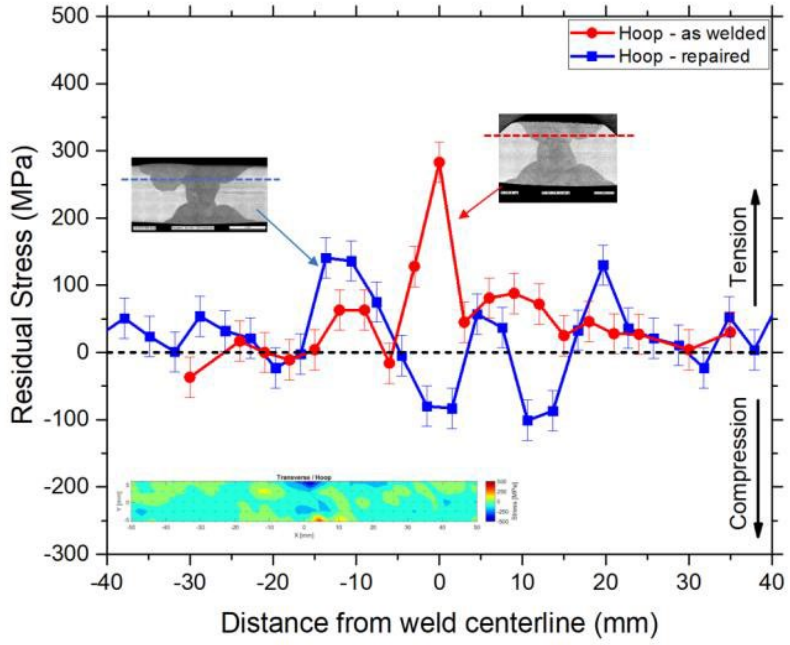

Figure 44 - Hoop WRS profiles perpendicular to the weld as AW and repaired specimens at the location of 3.3 mm from OD.

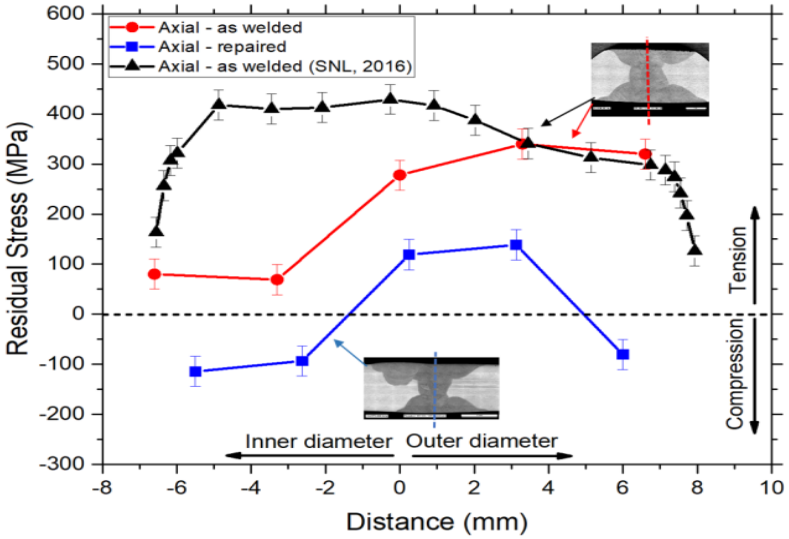

Figure 45 - Axial WRS profiles through thickness (parallel to the weld) for AW and repaired specimens at the original weld centerline.

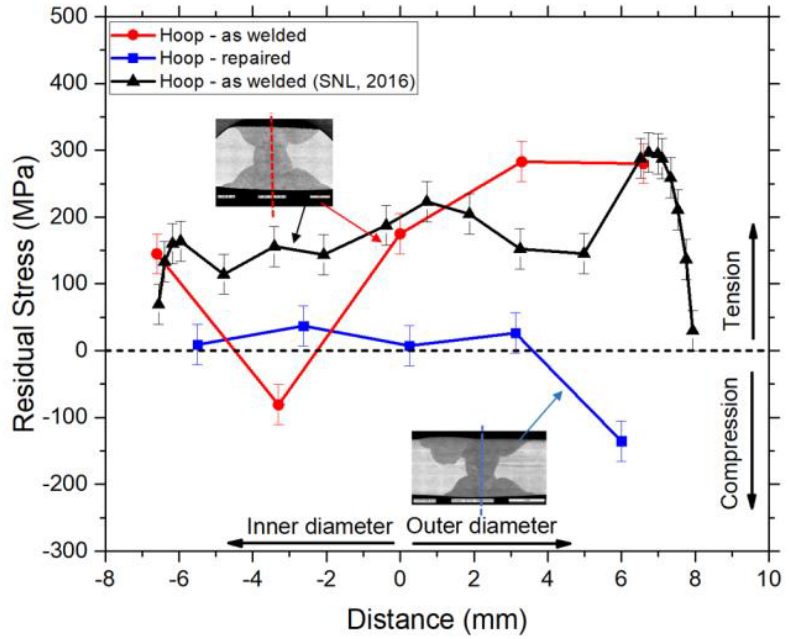

Figure 46 - Hoop WRS profiles through thickness (parallel to the weld) for AW and repaired specimens at the original weld centerline.

8. Residual Stresses in Spent Canisters with Friction Stir Welding Repair

Friction Stir Welding (FSW) – a solid state joining method with lower heat input, can be superior to the arc welding because heat input is usually less than that for the arc welding for most metals [32]. FSW has been considered to repair cracks in dry storage canisters. The process offers less degradation in the HAZ, less sensitization and low thermal distortion of the welded structures. In general, a rotating tool is passed along a pre-existing crack to heal it completely. Also during the tool traverse, a characteristic RS state is introduced into the weldment which may improve resistance to environmental degradation. Recently, PNNL [33] explored the feasibility of using FSW to repair cracks in austenitic SS plates and evaluate the process microstructure property correlations in the welded plates.

In the FSW repair study [33] at PNNL, hot-rolled, annealed and pickled plates of 304L SS were used with dimensions of 330 mm x 149 mm x 12.7 mm. The rolling direction of the plates was along the width. The EDM was used to introduce a seed crack lengthwise at the center of the plates. The crack was 0.33 mm wide with a depth of 5 mm. Single pass FSW was performed along the simulated cracks in order to repair them using the gantry-type TTI FSW machine at PNNL. The tool used is made of composite polycrystalline cubic boron nitride with a shoulder diameter of 36.8 mm and 5.7 long tool pin, see Figure 47(a). The weld speed was constant at 25.4 mm/min. The welding was carried out under a customized algorithm developed at PNNL, which can maintain the target temperature constant through varying tool rpm via a feedback mechanism at a user defined weld power. Two separated FSW weld tool temperatures were attempted at 725°C and 825°C, respectively. A tool tilt of -0.5° was used during the FSW at both temperatures. Figure 47(b) shows the picture of the post FSW plate at temperature of 725°C.

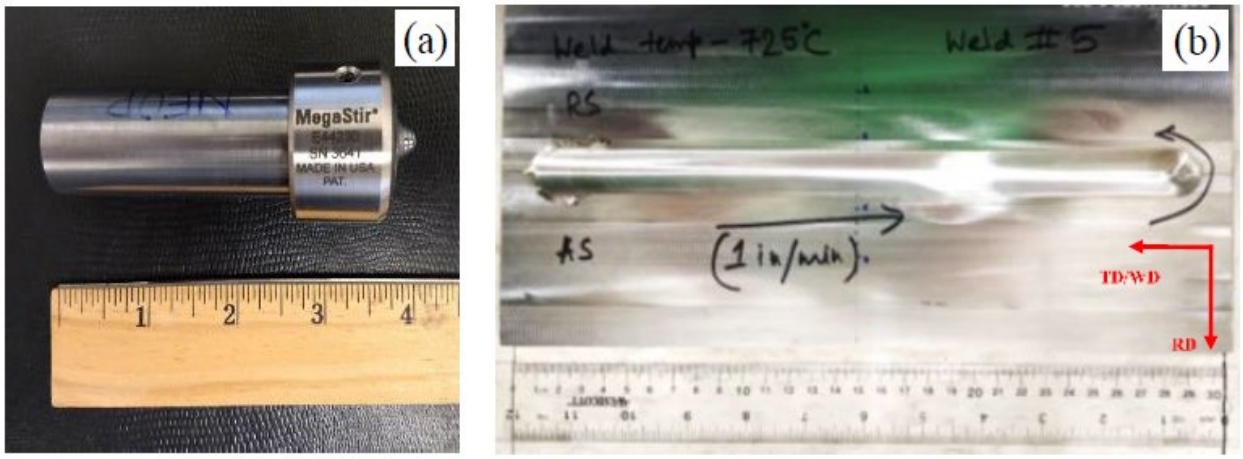

Figure 47- Illustration of FSW: (a) tool pin, and (b) 304L SS plate after FSW at 725°C [33].

The welded plates were tested ultrasonically to ensure that the simulated cracks have been healed completely through the thickness. For each temperature, the ultrasonic probe detected noise peaks close to the start and endpoint of the FSW runs. These noise peaks are indicative of the presence

of TW cracks. No noise peaks were noticed corresponding to the probe position other than the start and endpoint pointing complete healing of the stimulated crack along the total length.

Next, weld characterization was performed on small pieces sectioned at a plane perpendicular to the tool transverse direction. Microhardness profiles were obtained from base metal and across the weld with gauge length, width and thickness of 25.4 mm and 1.4 mm, respectively. Figure 48 shows the Vickers microhardness profile across the Stir Zone (SZ) of sample FSW weld at 725ºC.

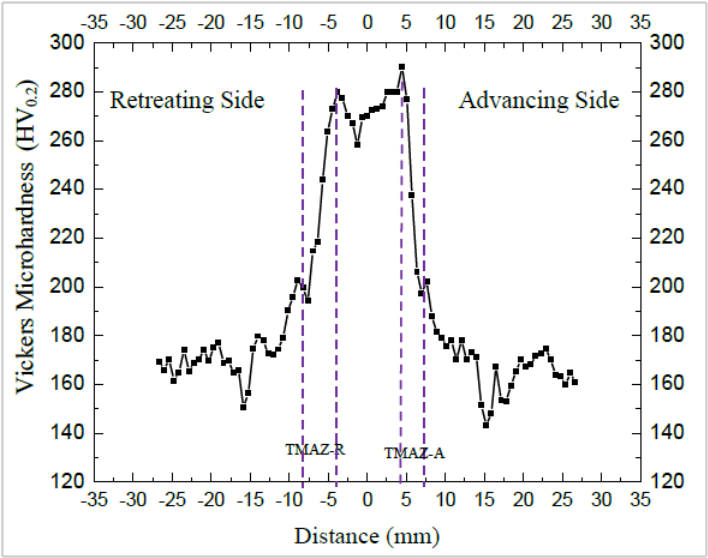

Figure 48 – Vickers microhardness profile across the SZ of sample FSW weld at 725ºC [33].

Uniaxial tensile tests were performed at room temperature with a strain rate of 10^{-3} /s. Figure 49 shows the engineering stress-strain curves of tensile test data. The YS of the BM is 310 MPa, whereas that of the 725ºC and 825ºC samples are 428 MPa and 440 MPa, respectively. The FSW samples show almost 100 MPa increase in the YS as compared to the BM. This is attributed to the grain refinement occurring in the SZ. This was balanced by a drop in ductility by a factor of 2. The BM elongation to fracture is 68%, the two FSW weld samples reduced to 28% and 30%, respectively. Only small increase in the UTS has been observed as compared to the BM. The UTS of the BM was 686 MPa, while the UTS of the two FSW weld samples are 690 MPa and 698 MPa, respectively.

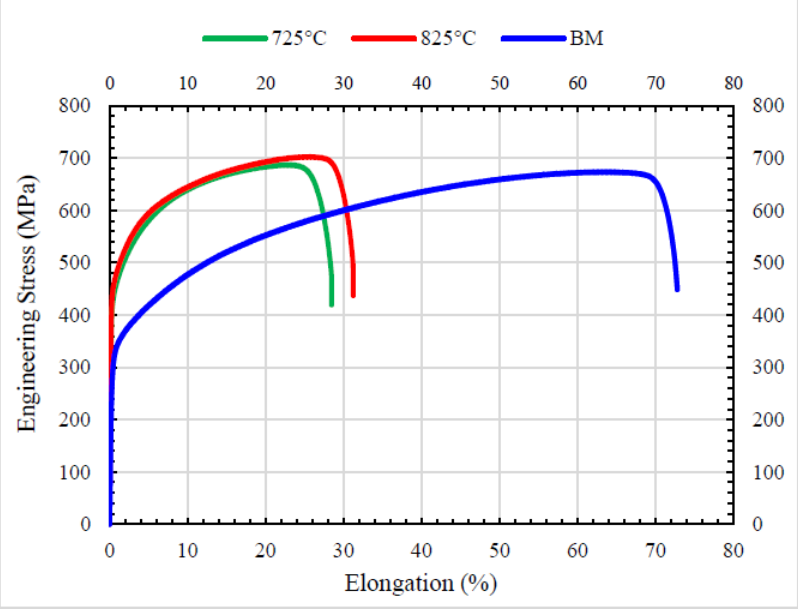

Figure 49 – Engineering stress-strain curves of the BM and Weld samples [33].

X-ray diffraction WRS measurement was performed across the weld along a line perpendicular to the weld direction. The points away from the weld are 5 mm apart while the interval was small (2 mm) close to and within the weld zone. Table 3 shows the WRS measurements obtained across the 825ºC SZ. Corresponding positions of the measurement points, retreating side (RS, only used for Table 3), advancing side (AS) and the welding direction are shown on the image next to the table. The residual stress components parallel and transverse to the weld direction are designated as σ_0 and σ_{90}, respectively. It is clear that the σ_{90} changes from tensile to compressive nature as one moves from the outside towards the SZ. This change occurs because of the stirring operation. However, the σ_0 component has remained tensile across the SZ. The measurements taken 25 – 30 mm away from the SZ-center show very high values of both the components indicating milling induced residual stress which did not actually get relieved. Further investigation is needed to understand this discrepancy.

In summary, microstructural observation showed significant grain refinement in the SZ as compared to the BM. Presence of flow lines or onion rings and Lazy-S structures were observed in both the SZ, and the difference of the onion ring size was noticed in the two SZs, which is attributed to different FSW tool rotation speeds. Compared to 725ºC FSW, grain size in the 825ºC SZ was found to be slightly larger, indicating further grain growth taking place at higher temperature and resulting in lower 825ºC SZ hardness. The mechanical properties of the weld samples were improved in terms of YS by almost 100 MPa. This was counterbalanced by a drop in percentage elongation to fracture.

In addition, PNNL [34] reported the updated results on investigations of viability of cold spray and FSW as a SNF dry storage canister mitigation tool, including the advantages and disadvantages of cold spray and FSW technologies as regarded the WRS for the canisters.

Table 3 – Residual stress values measured at positions across the 825°C FSW weld sample [33]

Distance from SZ-center (mm)	$\sigma_{0°}$ [MPa]	$\sigma_{90°}$ [MPa]
-30	645	674
-25	470	463
-20	274	243
-15	245	151
-13	294	200
-11	272	140
-9	157	-111
-7	131	-271
-5	159	-303
-3	167	-345
-1	157	-370
0	95	-394
1	152	-384
3	146	-400
5	143	-382
7	139	-306
9	141	-130
11	54	59
13	70	158
15	70	74
20	304	259
25	525	523
30	518	625

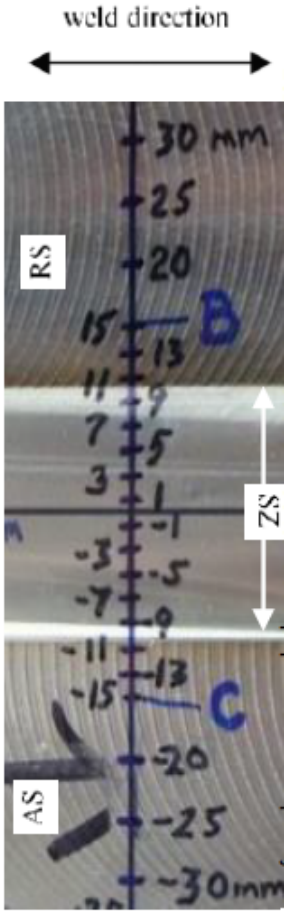

9. Discussion and Remarks

Various approaches for determination of WRS for as-welded canisters, for post-weld treatment methods for reducing the WRS, and for repair approaches for repairing cracks in the welds of canisters and reducing WRS for canisters have been reviewed. Below is a succinct listing of the information in this report.

9.1. Residual stress determination for as-welded canisters

For the as-welded canisters, the following methods can be used to determine the WRS:

- API 579 Estimation procedures;
- FEA simulation, including thermal and stress simulations;
- Experimental measurements, using DHD, neutral diffraction, and contour methods.

9.2. Post-weld treatments to reduce residual stresses for canisters

To reduce or relieve the WRS in the welds of canisters, the following technologies on post-weld treatments may be applied on the arc welds in canisters:

- Cold spray;
- Laser peening;
- Local post-weld heat treatment.

9.3. Repair approaches to reduce residual stresses for canisters

The following repair approaches can be used to repair cracks occurred in the welds and to reduce residual stresses in canisters:

- Fusion welding technology;
- Friction stir welding.

9.4. Suggestion of other repair technologies to reduce residual stresses

In order to reduce or redistribute the WRS in the canisters, some other repair technologies other than those discussed above include:

- Shot peening;
- Rolling;
- Ultrasonic impact treatment;
- Sleeve reinforcement;
- Mechanical patch.

These technologies used for other industry have not been evaluated in detail in this report.

10. Recommendations

A variety of technical approaches have been taken for determining the WRS and for effecting reduced stresses from from the as-welded SNF canisters. Non-welding repair methods such as cold spray show good promise as being a viable repair method to cover a crack and stop its growth. However, the structural acceptance of such a repaired canister, to be equivalent to an as-fabricated canister, has not been demonstrated. Evaluation of cold-sprayed canisters for structural acceptance would be part of the present ASME code case development for canister repair.

The additional following topics for canister advanced joining, WRS estimation, flaw tolerance evaluation, post-fabrication-weld treatment, and repair approaches are also suggested for further investigation.

10.1. **Optimize the arc welding technology to reduce WRS in canisters**

Arc welding technologies have been developed and used for fabrication of SNF canisters for many years. Welding technology has improved, and some low heat-input welding processes were developed in other industries for achieving low WRS and high weld metal strength/toughness. These new welding technologies could be adapted for fabricating SNF canisters with low WRS welds. In turn, this will significantly reduce the possibility of crack formation at the welds in canisters.

10.2. **Develop improved methods to estimate WRS for canisters**

The WRS in as-welded canisters can be measured using the experimental methods or obtained using the FEA simulations. However, both methods are time consuming, and can determine WRS only for case-by-case configurations. In contrast, an engineering estimate method is more effective and attractive, and able to develop a general procedure to estimate WRS for canisters using API 579 procedures. In order to obtain more accurate WRS for as-welded canisters, further investigation is recommended to optimize the factors required for the WRS estimation, including welding parameters and steel strength and toughness.

10.3. **Develop a fitness-for-service method tool for assessing canister flaw tolerance**

SRNL has developed an engineering approach for evaluating the canister integrity using the guidelines of API 579. This estimate approach adopted the table values of the stress intensity factors (or K factors) to determine the K factor solution using the complicated equations in API 579 for thick-wall cylinders, and the K factor-based failure assessment diagram (FAD) was employed for determining a crack instability criterion. However, most SNF canisters are thin-wall cylinders with a D/t >100, and thus a thin-wall estimate equation can be used to simplify the K factor calculation and to determine the K factor solutions for TW or PTW cracks with sufficient accuracy.

In addition, API 579 provides the tabular values of the K factors, rather than a closed-form function, because the tabular data of the K factors were obtained from extensive FEA

calculations for three variables, that is, the radius to wall thickness (R/t) ratio, the crack depth to wall thickness (a/t) ratio, and the crack aspect (a/c) ratio. To use the tabular values of the K factors, a three-parameter interpolation is required. In general, the interpolation calculation is inconvenient to use for an arbitrary crack instability analysis or a crack growth analysis. Closed-form solutions of the K factors are thus needed, but not available yet due to the difficulty of three-parameter regression. Using machine learning technology, the data-driven closed-form solutions of the K factors could be easily determined for different crack types, including axial and circumferential TW cracks and the outside and inside surface cracks. With the machine learning models of the K factors, the crack instability analysis and the crack growth analysis will become much simpler in terms of the K-based fracture mechanics method.

With use of the simplified thin-wall cylindrical solutions for estimating the K factors and the machine learning models of the K factors based on API 579 tabular data, an improved crack assessment method could be developed for consideration of WRS in as-received canisters. Furthermore, an Excel or Matlab software-based crack assessment tool can be developed if needed that can be easily used for assessing canister integrity.

10.4. **Evaluate new post-weld treatment approaches to reduce WRS for canisters**

Among the post-weld treatments to mitigate the WRS in as-welded canisters, the cold spray technology has been investigated by several different organizations. Compared to the cold spray, laser peening and local PWHT technologies have not been studied extensively for application to the SNF canisters. Research has demonstrated that these two methods may reduce the WRS in the canisters. However, local PWHT would be inconvenient to use for the large welds in the canisters. In contrast to this, the laser peening may be a promising technology that can be easily applied to the large welds in the canister. The laser peened welds may have compressive stresses on the peened layer of the welds in canisters.

10.5. **Develop new repair approaches to repair cracks and reduce WRS for canisters**

Friction stir welding has been investigated as a method for repairing cracks in the welds of SNF canisters. To apply FSW to an in-service canister is inconvenient, and a special FSW system would need to be developed.

Some crack repair methods commonly used in the pipeline industry may be appropriate to extend to repair cracks in canisters, such as mechanical patches and reinforced sleeves to be welded on the canisters. In addition to these crack repair methods, the cold spray and laser peening, which were developed for the post-weld treatment to mitigate the WRS in the as-welded canisters, may also be applied to eliminate the redistributed WRS near a crack in canisters after repair by a small patch or a large reinforced-sleeve.

11. References

[1] Kosaki A., SCC propagation rate of type 304, 314L steels under oceanic air environment, ASME *14th International Conference on Nuclear Engineering*, July 17-20, 2006, Miami, Florida, USA; Paper No. ICONE 14-89271.

[2] Tani J. Mayuzumi M., Arai T., Hara N., Stress corrosion cracking growth rates of candidate canister materials for spent nuclear fuel storage in chloride-containing atmosphere, *Materials Transaction*, Vol. 48(6), 2007: 1431-1437.

[3] Oberson G., Dunn D., Mintz T., et al., US NRC-sponsored research on stress corrosion susceptibility of dry storage canister, Materials in Marine Environments Conference (WM2013), February 24-28, 2013, Phoenix AZ, USA; Paper No. 13344.

[4] Chu S., *Flaw Growth and Flaw Tolerance Assessment for Dry Cask Storage Canisters*, Electric Power Research Institute, Palo Alto, CA, EPRI Report No. 3002002785.

[5] Lam P.S. and Sindelar R.L., Flaw stability considering residual stress for aging management of spent nuclear multiple-purpose canisters, *Journal of Pressure Vessel Technology*, Vol. 138, 2015: 041406.

[6] Section XI ASME Boiler and Pressure Vessel Code Case N-860, 2019 ASME Code Cases: Nuclear Components, Supplement 6, Approved July 6, 2020.

[7] Broussard J.E., Technical basis summary for code case N-860: Inspection requirements and evaluation standards for spent nuclear fuel storage and transportation containment systems, *Proceedings of the ASME Pressure Vessels and Piping Conference*, July 13-15, 2021, Virtual, Online, PVP2021-64176.

[8] ASME Boiler and Pressure Vessel Code (BPVC), Section XI, *Rules for Inservice Inspection of Nuclear Power Plant Components*, American Society of Mechanical Engineering, New York, USA, 2020.

[9] HOLTEC International, September 6, 2002, "HOLTEC International Final Safety Analysis Report for the HI-STORM Cask System," HI-2002444, Marlton, New Jersey

[10] API 579-1 / ASME FFS-1, *Fitness-for-Service*, American Petroleum Institute, Washington, DC, USA; 2016.

[11] Lam P.S., Sindelar R.L., Duncan A.J., Adams T.M., A framework to develop flaw acceptance criteria for structural integrity assessment of multipurpose canisters for extended storage of used nuclear fuel, *Proceedings of ASME Pressure Vessels and Piping Division Conference*, July 20-24, 2014, Anaheim, California, USA.

[12] Lam P.S. and Sindelar R.L., Development of flaw acceptance criteria for aging management of spent nuclear fuel multiple-purpose canisters, *Proceedings of ASME Pressure Vessels and Piping Division Conference*, July 19-23, 2015, Boston, Massachusetts, USA.

[13] Shi J., Wei L., Lam P.S., Flaw stability analysis of semi-elliptical surface cracks in canisters under the influence of welding residual stress, *Proceedings of ASME Pressure Vessels and Piping Division Conference*, July 17-21, 2016, Vancouver, British Columbia, Canada.

[14] EDF Energy Nuclear Generation Ltd, Assessment of the Integrity of Structures containing Defects, R6 Revision 4, December 2014.

[15] Lam P.S., Sindelar R.L., Duncan A.J., Carter J.T., Bounding surface flaw configuration susceptible to stress corrosion cracking under welding residual stress in a multiple-purpose canister, *Proceedings of ASME Pressure Vessels and Piping Division Conference*, July 16-20, 2017, Waikoloa, Hawaii, USA.

[16] Enos D.G. and Bryan C.R., *Characterization of Canister Mockup Weld Residual Stresses*, Final Report, FCRD-UFD-2016-00064, Sandia National Laboratories, November 2016.

[17] Newman J.C. and Raju I.S., *Stress Intensity Factor Equations for Cracks in Three-Dimensional Finite Bodies Subjected to Tension and Bending Loads*, NASA Technical Memorandum 86793, NASA Langley Research Center, Hampton, VA, 1984.

[18] Lam P.S., et al., Stress corrosion cracking of carbon steel weldments, *Proceedings of ASME Pressure Vessels and Piping Division Conference*, July 17-21, 2005, Denver, Colorado, USA.

[19] Gim J.M., Kim, J.S., Kim Y.J., Lam P.S., FE welding residual stress analysis and validation for spent nuclear fuel canisters, *Proceedings of ASME Pressure Vessels and Piping Division Conference*, July 15-20, 2018, Prague, Czech Republic.

[20] Lee H.J., Kim Y.J., Lam P.S., Sindelar R.L., Engineering J estimates for spent fuel canisters under combined mechanical and welding residual stresses, *Proceedings of ASME Pressure Vessels and Piping Division Conference*, July 14-19, 2019, San Antonio, Texas, USA.

[21] Wu X., On residual stress analysis and microstructural evolution for stainless steel type 304 spent nuclear fuel canisters weld joint: Numerical and experimental studies, *Journal of Nuclear Materials*, Vol. 534, 2020: 152131.

[22] Duncan A.J., Lam P.S., Sindelar R.L., CISCC experiment of a large plate sectioned from a spend nuclear fuel canister, *Proceedings of ASME Pressure Vessels and Piping Division Conference*, August 3, 2020, Virtual, Online.

[23] Lam P.S., Duncan A.J., Sindelar R.L, Bryan C.R., *Large Plate Experiment of Chloride-Induced Stress Corrosion Cracking in Spent Nuclear Fuel Storage Canisters*, Technical Report SRNL-STI-2020-00315, September 5, 2020.

[24] Lam P.S. and Kim Y.J., *Flaw Stability and Stress Corrosion Cracking of Austenitic Stainless Steel Canisters for Long Term Storage and Transportation of LWR Used Fuel*, I-NERI Project Number 2016-001-K, US Department of Energy, Office of Nuclear Energy, Washington, D.C., USA, 2016.

[25] Tatman J., *Welding and Repair Technology Center: Residual Stress Analysis of Cold Spray Deposition for Stress Corrosion Cracking Mitigation and Repair* – Technical Report # 3002018449, EPRI, Palo Alto, CA; August 2020.

[26] Ross K, Jiang H., Alabi M., Enderlin C., *Investigation of Cold Spray as a Dry Storage Canister Repair and Mitigation Tool*, DOE Report by Pacific Northwest National Laboratory, September 30, 2020.

[27] Hackel L., Rankin J., Walter M., et al., Preventing stress corrosion cracking of spent nuclear fuel dry storage canisters, *Procedia Structural Integrity*, Vol. 19, 2019: 346-361.

[28] Ren Y., et al., Residual stress state of X65 pipeline birth welds before and after local and furnace post weld heat treatment, *Journal of Pressure Vessel Technology*, Vol. 139, 2017: 041401.

[29] Wang J.A., Payzant A., Bunn J., An K., *Neutron Residual Stress Mapping for Spend Nuclear Fuel Storage Canister Weldment*, Technical Report ORNL/TM-2018/827, Oak Ridge National Laboratory, April 20, 2018.

[30] Chatzidakis S., Tang W., Chen J., Miller R., Payzant A., Bunn J., Wang J.A., Neutron residual stress mapping of repaired spend clear fuel welded stainless steel, *International High-Level Radioactive Waste Management* (IHLRWM 2019), April 14-18, 2019, Knoxville, TN, USA.

[31] Chatzidakis S., Tang W., Miller R., Payzant A., Bunn J., Bryan C., Scaglione J., Wang J.A., Neutron diffraction illustrates residual stress behavior of welded alloys used as radioactive confinement boundary, *International Journal of Pressure Vessel and Piping*, Vol. 191, 2021: 104348.

[32] Lienert T.J., Stellwag W.L., Lehman L.R., Comparison of heat inputs: Friction stir welding vs. Arc welding, *American Welding Society Conference*, 2002.

[33] Bhattacharyya M., Charit I., Raja K., Darsell J., Jana S., A feasibility study on crack repair in austenitic stainless steel dry storage canisters using isothermal friction stir welding, *Proceedings of the ASME Pressure Vessels and Piping Conference*, August 3, 2020, Virtual, Online, PVP2020-21716.

[34] Ross K. and Alabi M., *Update on Investigations of Viability of Cold Spray and FSW as Spent Nuclear Fuel Dry Storage Canister Mitigation Tool*, Technical Report PNNL-29217, Pacific Northwest National Laboratory, September 30, 2019.